Geophys. J. R. astr. Soc. (1985) **80**, 387–417

A WKBJ spectral method for computation of *SV* synthetic seismograms in a cylindrically symmetric medium

Chang-Eob Baag and Charles A. Langston *Department of Geosciences, The Pennsylvania State University, University Park, Pennsylvania 16802, USA*

Accepted 1984 August 6. Received 1984 July 9; in original form 1984 February 17

Summary. A method of synthetic seismogram computation for teleseismic *SV*-waves is developed in order to treat quantitatively *SV*-waves in problems of body wave source inversion and source–receiver structure studies. The method employs WKBJ theory for a generalized ray in a vertically inhomogeneous half-space and the propagator matrix technique for waves in near-surface homogeneous layers. Wavenumber integration is done along the real axis of the wavenumber plane and anelasticity is included by using complex velocity in all regions of the earth model. The near-surface source structure is taken into account in the computation for the case of the shallow source by allowing a point source to be located in the homogeneous layers. Source and receiver area structures are also allowed to differ. A general moment tensor point source is considered.

Introduction

SV-waves have received little attention from seismologists in comparison to studies of *P*-, or even *SH*-, waves. This is due to the relatively complex nature of *SV*-wave propagation where receiver *Sp* conversions and shear-coupled *PL*-waves serve to obscure the direct *SV* arrival. Furthermore, they are poorly understood from a wave propagation standpoint. These facts make it difficult to use the *SV*-wave in standard travel-time studies and in detailed source mechanism studies. However, *SV*-waves potentially contain as much source information as *P*- or *SH*-waves from earthquakes and explosions, and they should be usable in earth structure studies in much the same ways as the other phases. The non-isotropic explosion problem (e.g. Langston 1983; Masse 1981) could benefit from the inclusion in source modelling studies of long-period *SV* data. Where observable, long-period *SV*-waves are intermediate in frequency content between the relatively short-period *P*-wave and long-period surface waves. Seismic anisotropy in earth structure (Crampin 1977; Ando, Ishikawa & Yamazaki 1983) may also be investigated by the combined use of *SV* and *SH* in waveform studies of upper mantle structure. In order to treat quantitatively the *SV*-wave in problems of body wave source inversion and source–receiver structure studies, synthetic seismogram computation for *SV*-waves is necessary.

There are a variety of approaches available for the computation of body waves propagating in stratified media. Following Chapman's (1978) divisions, these may be classified as slowness methods or spectral methods, depending on the order in which inverse transforms are performed. The slowness method includes generalized ray theory or Cagniard–deHoop methods which are useful when only a relatively small number of generalized rays are needed to build the solution of interest. Ray solutions may be exact (e.g. Pekeris, Abramovici & Jarosch 1965; Helmberger 1968; Wiggins & Helmberger 1974) or be composed of a suitable approximation (Mellman & Helmberger 1978; Chapman 1978) of sufficient accuracy for a particular problem. Spectral methods include the reflectivity method of Fuchs & Müller (1971) and Kind (1978), direct numerical integration (Kennett & Kerry 1979; Kennett 1980; Apsel 1979; Wang & Herrmann 1980; Bouchon 1981), the locked mode method of Harvey (1981), and the 'full wave' method of Cormier & Richards (1976, 1977), Choy (1977), and Cormier (1980). The principal drawback of using most spectral methods for body wave computations lies in the high cost involved in the many layer matrix computations needed when parameterizing velocity gradients by many discrete horizontal layers. Several authors, notably Frazer (1977), Woodhouse (1978), Chapman (1978), Cormier & Richards (1976, 1977), and Cormier (1980) have suggested the use of WKBJ or uniform asymptotic expansions to compute the effect of waves propagating in layers with smooth velocity functions. These approximations effectively reduced computation time by avoiding the fine layering needed to represent a velocity gradient.

Frazer's (1977) work is of direct importance to this study and motivates many of the approaches used here. He reduced the computational time in the synthesis of teleseismic *SV*-waves by using the Langer (1949) approximation in the radial wave functions for a generalized ray with a turning point in the mantle, and the spherical layer matrix in the crust. His theoretical formulation is especially convenient for the investigation of *P*-wave velocity gradients below the Mohovoričić discontinuity. Unfortunately, the method neither included the effect of near-source structure on *SPL*-wave excitation for shallow sources, nor anelastic attenuation.

In order to overcome some of the limitations of previous methods for synthesis of *SV*-waves, and to provide more realistic interpretations of the seismogram, a comprehensive method of synthetic seismogram computations for teleseismic *SV*-waves is developed in the current study. The theory is formulated for vertically inhomogeneous earth structure in a cylindrical coordinate system (Fig. 1). Spherical models are incorporated by using an Earth-flattening transformation which produces the equivalent vertically inhomogeneous model (Müller 1971, 1977; Chapman 1973; Gilbert & Helmberger 1972). The method employs WKBJ theory for a 'generalized' ray in a vertically inhomogeneous half-space and the propagator matrix technique for waves in near-surface homogeneous layers (Fig. 2). Because teleseismic *SV*-waves are heavily influenced by the crust and upper mantle, the propagator matrix technique is applied to these regions allowing multiple reflections and conversions of *P*–*S*-wave phases in layers. The *Sp*-diffraction which is initially set up at the Moho is under the computational control of the matrix formulation. The scheme of the WKBJ ray in the structure below the low-velocity zone down to the lower mantle reduces the computational time significantly. Anelasticity is included by using complex valued velocity in all regions of the earth model.

We show in the companion paper (Baag & Langston 1985) that the effect of near-surface source structure is important for *SV* and *SPL* generated from a shallow source, since large reverberations of *P*- and *S*-wave types leak into the mantle as *SV*-waves. This near-surface source structure is included in the calculation for the case of shallow sources by allowing a point source to be located in the upper layers with appropriate discontinuities in stress

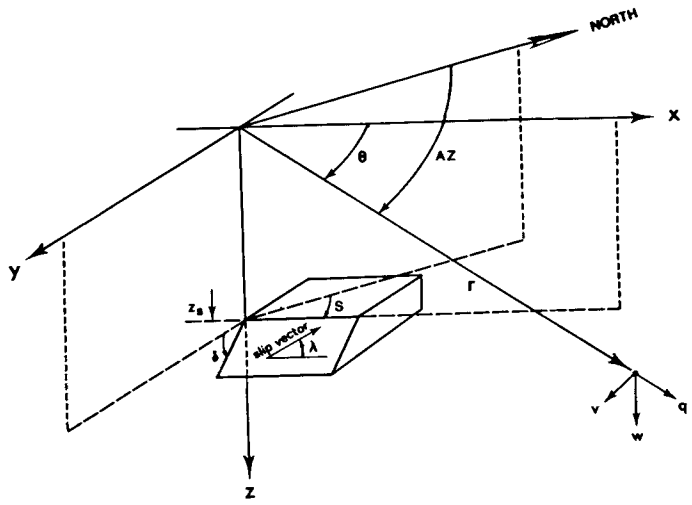

Figure 1. Coordinate systems and conventions.

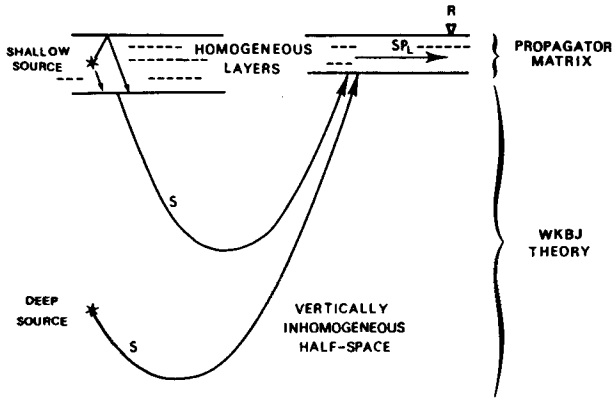

Figure 2. Schematic diagram for excitation of *SPL*-waves by deep and shallow sources, and the mathematical techniques used in formulating the theory.

and displacement at the source depth (Fig. 2). The downgoing *SV*-wave potential in the half-space is evaluated using propagator matrix techniques and then is converted to the WKBJ potential for a turning wave. The upgoing wave at the receiver interacts with receiver structure. The WKBJ potential of the upgoing wave, evaluated at the half-space boundary in the receiver structure, is transformed to the potential coefficient used in the propagator matrix to generate the response for the near-surface receiver structure. The source and receiver structure are allowed to be different, since the *SPL*-wave is seen to be generated near the receiver but the radiated *SV*-wave near the source is strongly affected by source structure particularly for a shallow source.

The solution is evaluated in the frequency domain by evaluating a wavenumber integral over a specified range of real-valued wavenumbers, and the result is inverse Fourier-transformed to get displacement at the free surface in the time domain.

WKBJ formulation for an inhomogeneous half-space

The approximate Green's function, G_{ij}, for the directional point force with delta function time and unit strength is given by (see Appendix A)

$$G_{ij} = \frac{1}{4\pi\omega^2 \rho^{1/2}(z_s)\,\rho^{1/2}(z)} \left[\frac{\partial^2}{\partial x_i \partial x_j} [A_\beta - A_\alpha] + \frac{\omega^2}{\beta^2(z)} A_\beta \delta_{ij} \right] \tag{1}$$

where A_α and A_β are Sommerfeld-like integrals of the WKBJ solution given by

$$A_\alpha = \int_0^\infty \frac{k \exp\left[\mp \int_{z_s}^{z} \nu_\alpha(x)\,dx \right]}{\nu_\alpha^{1/2}(z_s)\,\nu_\alpha^{1/2}(z)} J_0(kr)\,dk \tag{2}$$

$$A_\beta = \int_0^\infty \frac{k \exp\left[\mp \int_{z_s}^{z} \nu_\beta(x)\,dx \right]}{\nu_\beta^{1/2}(z_s)\,\nu_\beta^{1/2}(z)} J_0(kr)\,dk$$

for P- and S-waves respectively. Here, $\nu_\alpha(z) = i\omega(1/\alpha^2(z) - 1/c^2)^{1/2}$, and $\nu_\beta(z) = i\omega(1/\beta^2(z) - 1/c^2)^{1/2}$. z is the depth, z_s the source depth, r the horizontal distance, k the horizontal wavenumber, ω the angular frequency. $\rho(z)$, $\alpha(z)$, $\beta(z)$ are the density, and the velocities of the compressional and the shear waves. x_i, x_j, $J_0(kr)$, δ_{ij} are the components of the coordinates, Bessel function of order zero, and Kronecker delta symbol, respectively.

In order to get solutions for various dislocation sources, the displacement discontinuity term of the representation theorem for inhomogeneous media is used

$$u_i(\bar{x}) = \iint_{s'} [u_j(\bar{x}')]\, C_{jkpq}(\bar{x}')\, n_k \frac{d}{dx'_q} G_{ip}(\bar{x}, \bar{x}')\,ds' \tag{3}$$

where the prime indicates source coordinates, $[\bar{u}_j(x')]$ is the displacement discontinuity, C_{jkpq} are elastic constants, and n_k is the surface unit vector (Burridge & Knopoff 1964).

By using displacement-potential equations (Langston & Helmberger 1975; Harkrider 1976) with the modification of a factor of $\rho^{-1/2}(z_s)$ in the cylindrical coordinate system, the potentials of the three types of dislocation cases are obtained. The results for shear wave potentials are as follows:

$$\psi_1(r, \theta, z, \omega) = \frac{\mu D(\omega)}{4\pi\omega^2 \rho^{1/2}(z_s)} \int_0^\infty \epsilon \nu_\beta F_\beta J_2(kr)\,dk\,A_1$$

$$\psi_2(r, \theta, z, \omega) = \frac{\mu D(\omega)}{4\pi\omega^2 \rho^{1/2}(z_s)} \int_0^\infty \left[\frac{(k_\beta^2(z) - k^2)}{k} \frac{\nu_\beta(z_s)}{\nu_\beta(z)} - k \right] F_\beta J_1(kr)\,dk\,A_2$$

$$\psi_3(r, \theta, z, \omega) = \frac{\mu D(\omega)}{4\pi\omega^2 \rho^{1/2}(z_s)} \int_0^\infty \epsilon [\nu_\beta(z) + 2\nu_\beta(z_s)]\, F_\beta J_0(kr)\,dk\,A_3. \tag{4}$$

Here

$$F_\beta = \frac{k \exp[G_\beta(z)]}{\nu_\beta^{1/2}(z_s)\,\nu_\beta^{1/2}(z)}$$

$$G_\beta(z) = \mp \int_{z_s}^{z} \nu_\beta(x)\, dx, \qquad \begin{cases} (-): \text{ for downgoing waves} \\ (+): \text{ for upgoing waves} \end{cases}$$

$$\epsilon = \begin{cases} + & \text{for downgoing waves} \\ - & \text{for upgoing waves.} \end{cases}$$

ψ_1, ψ_2, ψ_3 are SV-wave potentials for vertical strike-slip, vertical dip-slip, and 45° dip-slip dislocation source cases, respectively. A_1, A_2, and A_3 are the corresponding source orientation terms (Langston & Helmberger 1975). μ is the shear modulus at the source, and $D(\omega)$ the Fourier transformed dislocation time function.

In the derivations of these potentials, the approximations

$$\begin{aligned} \frac{\partial F_\beta}{\partial z} &= -\epsilon \nu_\beta(z) \left[1 + 0\left(\frac{1}{\omega}\frac{d\nu}{dz}\right)\right] F_\beta \doteq -\epsilon \nu_\beta(z) F_\beta \\ \frac{\partial F_\beta}{\partial z'} &= \epsilon \nu_\beta(z_s) \left[1 + 0\left(\frac{1}{\omega}\frac{d\nu}{dz}\right)\right] F_\beta \doteq \epsilon \nu_\beta(z_s) F_\beta \end{aligned} \tag{5}$$

were used.

When the WKBJ downgoing wave eventually turns, its amplitude is modified, and the ratio of amplitude of the upgoing wave to the downgoing wave is defined as a reflection coefficient. This reflection coefficient is obtained by using Stoke's equation and its Airy function solution assuming linear dependence of the square of vertical slowness, $\eta^2(z)$, on z around the turning point (Budden 1961). The result is

$$R = i \operatorname{sgn}(\omega) \exp\left[-2 \int_{z_s}^{z_p} \nu(x)\, dx\right]. \tag{6}$$

z_p is the turning point of a ray such that the vertical slowness $\eta(z) = 0$. If the depth z is real and $\eta(z)$ is a real-valued function, this equation has a real-valued zero, i.e. a real value of turning point. If intrinsic attenuation is introduced through complex-valued velocity, the effective velocity becomes (Schwab & Knopoff 1972)

$$\frac{1}{v_e(z)} = \frac{1}{v(z)}\left[1 - \frac{i}{2Q(z)}\right] \tag{7}$$

where $Q(z)$ is the slowly varying, depth-dependent, and frequency-independent seismic quality factor. With this effective velocity the square of vertical slowness, $\eta^2(z)$, has no real-valued zero, i.e. no turning point in real-falued depth, since it is a complex-valued function

$$\eta^2(z) = \frac{1}{v^2(z)}\left[1 - \frac{1}{4Q^2(z)}\right] - \frac{1}{c^2} - i\frac{1}{v^2(z)\,Q(z)}. \tag{8}$$

However, in reality there are still turning points even where intrinsic attenuation exists. It is useful to introduce complex-valued depth, $z = x + iy$, to find the turning point. The analytical solution of $\eta(z) = 0$ is not easy, since the separation of real and imaginary parts of the function $\eta^2(z)$ with complex-valued depth z is very complicated. A good way to find the solution is to find the position in the complex z plane of the minimum of the absolute value of $\eta^2(z)$ numerically instead of finding the exact position of the zeros. This can be done by moving a diamond-shaped searching net consisting of five points over a finely-

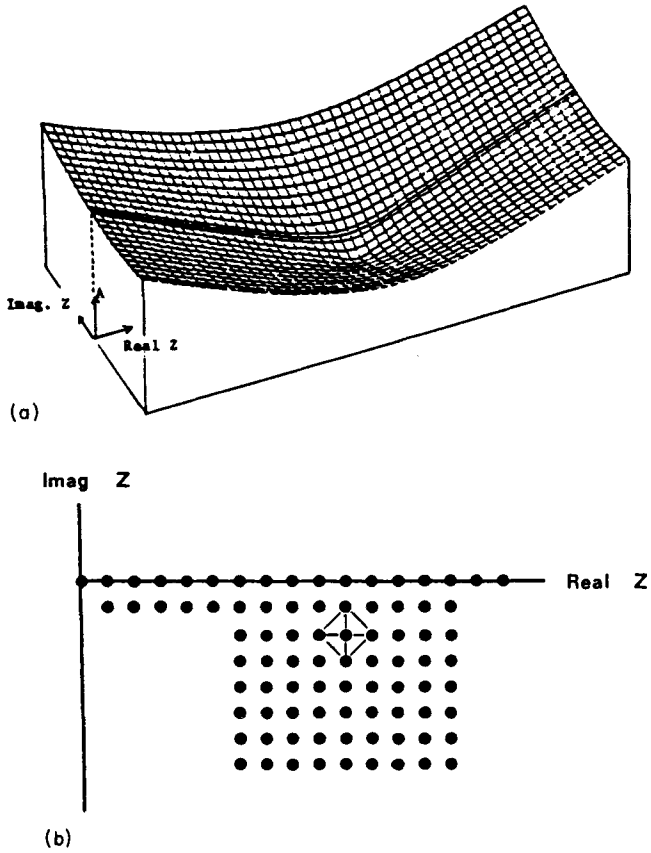

Figure 3. Location of the complex-valued turning point of WKBJ ray. (a) Plot of absolute value of the square of vertical slowness. (b) Moving diamond-shaped searching net on complex-valued depth plane.

divided grid in the complex z plane (Fig. 3). The centre part of the net is the turning point when it has a minimum value among the surrounding four points. This technique is valid because a single turning point is allowed and the function of absolute value of $\eta^2(z)$ is a monotonically decreasing and increasing function, respectively, on the opposite sides of the minimum point (Fig. 3). The depth integral of $\nu(z)$ in the equation (6) is done along a contour to the complex-valued turning point. The contour follows the real z-axis first and then a parallel to the imaginary axis connecting the turning point.

By assuming that $v(z)$ and $Q(z)$ vary linearly with depth around the turning point, or

$$\begin{aligned} v(z) &= v_0 + v_1 z \qquad (v_1 z)/v_0 \ll 1 \\ Q(z) &= Q_0 + Q_1 z \qquad (Q_1 z)/Q_0 \ll 1, \end{aligned} \tag{9}$$

the square of vertical slowness can be shown by the method of successive approximations to be $\eta^2(z) \sim h_0 + h_1 z$. This satisfies the linearity of $\eta^2(z)$ in Stoke's equation. Here h_0 and h_1 are complex numbers.

Propagator matrix method for the near-surface region

The treatment of waves propagating in the near-surface region of homogeneous layers is straightforward and follows the developments of Thomson (1950), Haskell (1953, 1960,

1962) and Harkrider (1964). The numerical problem of machine accuracy in evaluating the wave solution in terms of propagator matrices has been discussed by many investigators (e.g. Knopoff 1964; Dunkin 1965; Abo-Zena 1979). We apply Watson's (1970) reduced compound matrix formulation in computations of the layer matrix to avoid the problem and get faster machine computation.

A wave from a source in a stack of layers arrives at the half-space, and it is assumed to propagate through the inhomogeneous half-space as a WKBJ turning shear wave. The downgoing *S*-wave potential coefficient of the wave transmitted from the stack of layers at the half-space boundary is needed in order to convert the wave into a WKBJ form. Here a coefficient is presented which is very efficient in numerical calculation.

The derivation of the relation between surface displacement and the wave coefficients in the half-space is given in detail by Harkrider (1964).

$$\begin{bmatrix} \hat{\Delta}'_n \\ \hat{\Delta}'_n \\ \hat{\omega}'_n \\ \hat{\omega}'_n \end{bmatrix} = \mathbf{J} \left[\begin{pmatrix} \dot{u}_0/c \\ \dot{w}_0/c \\ 0 \\ 0 \end{pmatrix} + \begin{pmatrix} D_1 \\ D_2 \\ D_3 \\ D_4 \end{pmatrix} \right] \tag{10}$$

where $\mathbf{J} = \mathbf{E}^{-1}\mathbf{A}$ and

$$\mathbf{D} = \mathbf{A}^{a^{-1}} \begin{bmatrix} \delta_1 \\ \delta_2 \\ \delta_3 \\ \delta_4 \end{bmatrix}.$$

Here $\hat{\Delta}'_n$ and $\hat{\omega}'_n$ are normalized potential coefficients of downgoing *P*- and *S*-waves at the half-space. $\dot{u}_0$ and $\dot{w}_0$ are radial and vertical particle velocities at the free surface. $\mathbf{A}$ is Haskell's layer matrix. $\mathbf{E}^{-1}$ and $\mathbf{A}^{a^{-1}}$ are the inverse layer matrices at the half-space and above the source, respectively (Appendix B). The δ_i are components of the displacement discontinuity at the source depth (Harkrider 1964). These components for the explosion or the dislocation sources are given in Appendix B.

Of the four unknowns in equation (10), two solutions are given as (see Appendix B)

$$\begin{aligned} \frac{\dot{u}_0}{c} &= \frac{1}{R_{11}} [R_{13}D_3 + R_{15}D_4] - D_1 \\ \frac{\dot{w}_0}{c} &= -\frac{1}{R_{11}} [R_{12}D_3 + R_{13}D_4] - D_2. \end{aligned} \tag{11}$$

R_{ij} is the compound matrix element (Harkrider 1970; Appendix B) which is based on Dunkin's formulation (Dunkin 1965) of the second-order subdeterminant of the Haskell matrix.

$$R_{ij} = \bar{J} \begin{vmatrix} kl \\ mn \end{vmatrix} = \bar{J}_{km}\bar{J}_{ln} - \bar{J}_{kn}\bar{J}_{lm} \tag{12}$$

where i or j are the numbers 1, 2, 3, 4, 5, 6 which correspond to the pairs kl or mn = 12, 13, 14, 23, 24, 34 respectively. $\bar{J}_{ij}$ is the element of a 2 x 4 matrix produced by the subtraction of elements between rows of the $\mathbf{J}$ matrix (Appendix B).

From equations (10) and (11), we get the coefficient below the half-space boundary for *SV*-waves as

$$\hat{\omega}_n' = \frac{1}{R_{11}} [0, 0, (J_{31}R_{13} - J_{32}J_{12} + J_{33}R_{11}), (J_{31}R_{15} - J_{32}R_{13} + J_{34}R_{11})] \cdot \mathbf{A}^{a^{-1}} \begin{bmatrix} \delta_1 \\ \delta_2 \\ \delta_3 \\ \delta_4 \end{bmatrix}. \tag{13}$$

Even though this solution is concise, it poses problems in actual numerical calculations. All three types of matrix elements **J**, **R** and **A** are needed in each layer, and the product and subtractions of these matrix elements result in significant numerical errors. The following technique is used to circumvent these problems.

By separation of the elements $J_{ij}R_{kl}$ into half-space and layer portions

$$J_{ij}R_{kl} = \sum_m \sum_n E^{-1}_{im} A_{mj} R^{\mathrm{H}}_{kn} R^{\mathrm{L}}_{nl} \tag{14}$$

where superscripts H and L indicate half-space and layer, and with the definition of a new matrix **H** for the half-space (Appendix B)

$$[H_{21}, H_{22}, H_{23}, H_{24}] = [E^{-1}_{31}R^{\mathrm{H}}_{13} + E^{-1}_{33}R^{\mathrm{H}}_{11}, E^{-1}_{31}R^{\mathrm{H}}_{15}, E^{-1}_{31}R^{\mathrm{H}}_{16} - E^{-1}_{33}R^{\mathrm{H}}_{13}, -E^{-1}_{33}R^{\mathrm{H}}_{15}], \tag{15}$$

the coefficient is reformed to be

$$\hat{\omega}_n' = \frac{1}{R_{11}} [H_{21}, H_{22}, H_{23}, H_{24}] \begin{bmatrix} 0 & 0 & A_{11} & A_{12} \\ 0 & 0 & A_{21} & A_{22} \\ 0 & 0 & A_{31} & A_{32} \\ 0 & 0 & A_{41} & A_{42} \end{bmatrix} \mathbf{A}^{a^{-1}} \begin{bmatrix} \delta_1 \\ \delta_2 \\ \delta_3 \\ \delta_4 \end{bmatrix}. \tag{16}$$

The multiple matrix multiplications have been removed for the half-space and the layers below the source, but they still remain for the layers above the source.

By separation of the element A_{ij} into matrix elements below and above the source

$$A_{ij} = \sum_k A^{\mathrm{b}}_{ik} A^{\mathrm{a}}_{kj} \tag{17}$$

where superscript b and a indicate below and above the source, and by using Dunkin's second-order subdeterminant technique, we get the final result

$$\hat{\omega}_n' = \frac{1}{R_{11}} [H_{21}, H_{22}, H_{23}, H_{24}] \, \mathbf{A}^b \begin{bmatrix} R^a_{31} & -R^a_{21} & R^a_{11} & 0 \\ R^a_{51} & -R^a_{31} & 0 & R^a_{11} \\ R^a_{61} & 0 & -R^a_{31} & R^a_{21} \\ 0 & R^a_{61} & -R^a_{51} & R^a_{31} \end{bmatrix} \begin{bmatrix} \delta_1 \\ \delta_2 \\ \delta_3 \\ \delta_4 \end{bmatrix}. \tag{18}$$

This yields the complete separation of matrix types into half-space, layers-below, and layers-above the source with no double or triple multiplication of matrix elements in any one layer. This reduces the time of numerical computation and enhances the accuracy.

If a seismic wave from a vertically inhomogeneous half-space comes toward the surface as a direct or turning wave, it will eventually arrive at the layer–half-space boundary near

the receiver. By assuming that the potential coefficients of these waves under the stack of layers are known, the displacements at the Earth's surface can be easily calculated.

From the matrix equation of surface displacements and the half-space coefficients (Harkrider 1964)

$$\begin{bmatrix} \hat{\Delta}_n' + \hat{\Delta}_n'' \\ \hat{\Delta}_n' - \hat{\Delta}_n'' \\ \hat{\omega}_n' - \hat{\omega}_n'' \\ \hat{\omega}_n' + \hat{\omega}_n'' \end{bmatrix} = \mathbf{J} \begin{bmatrix} \dot{u}_0/c \\ \dot{w}_0/c \\ 0 \\ 0 \end{bmatrix} \tag{19}$$

the radial and vertical velocity at the surface is obtained as

$$\begin{bmatrix} \dot{u}_0/c \\ \dot{w}_0/c \end{bmatrix} = \frac{2}{R_{11}} \begin{bmatrix} \bar{J}_{22}, & -\bar{J}_{12} \\ -\bar{J}_{21}, & \bar{J}_{11} \end{bmatrix} \begin{bmatrix} \hat{\Delta}_n'' \\ \hat{\omega}_n'' \end{bmatrix}. \tag{20}$$

The vertical function of a wave potential in the formulation for the layer matrix can exponentially decay due to either a large value of ray parameter which results in a vertically inhomogeneous wave or to the seismic quality factor Q of anelastic attenuation. This property of decay appears mathematically in the form of complex number in the non-dimensional vertical slownesses r_α of a *P*-wave and r_β of an *S*-wave.

$$\begin{aligned} r_\alpha^2 &= \left(\frac{c}{\alpha_e}\right)^2 - 1 \\ r_\beta^2 &= \left(\frac{c}{\beta_e}\right)^2 - 1 \end{aligned} \tag{21}$$

where α_e and β_e are the effective velocities of *P*- and *S*-waves in attenuating media defined in equation (23). If we choose the functions

$$\begin{aligned} \phi_\alpha(z, t) &= \exp\,[i(\omega t - k r_\alpha z)] \\ \phi_\beta(z, t) &= \exp\,[i(\omega t - k r_\beta z)] \end{aligned} \tag{22}$$

as the vertical wave functions of *P*- and *S*-waves propagating downward in the positive z direction, the effective velocities in an anelastic medium can be represented by

$$\begin{aligned} \frac{1}{\alpha_e} &= \frac{1}{\alpha}\left[1 - i\frac{1}{2Q_\alpha}\right] \\ \frac{1}{\beta_e} &= \frac{1}{\beta}\left[1 - i\frac{1}{2Q_\beta}\right] \end{aligned} \tag{23}$$

which have negative signs for imaginary parts. Here, Q_α and Q_β are the seismic quality factors of *P*- and *S*-waves, respectively. With the definition of equations (22) as the wave propagating downard, the real parts of normalized vertical slownesses r_α and r_β should be positive for this propagation direction, and the imaginary components of them be negative

for diminishing amplitude at large depth. Therefore, the space that has positive real and negative imaginary values of the vertical slowness is taken as the physical Riemann sheet.

$$\begin{aligned} &\mathrm{Re}\,(r_\alpha),\ \mathrm{Re}\,(r_\beta) > 0 \\ &\mathrm{Im}\,(r_\alpha),\ \mathrm{Im}\,(r_\beta) < 0. \end{aligned} \tag{24}$$

Connection between the layer matrix method for homogeneous layers and WKBJ solution in a vertically inhomogeneous half-space

If a wave from a source in a stack of layers over an inhomogeneous half-space propagates into the half-space, the potential coefficients of the layer matrix formulation should be converted to the equivalent coefficient for the WKBJ solution in the half-space based on displacement and stress at the boundary. When the WKBJ wave from an inhomogeneous half-space enters into a stack of homogeneous layers, we again need a conversion formula between potential coefficients. In order to do this, a depth-dependent variable coefficient is introduced for WKBJ potentials.

There is no unique way to define a variable coefficient and its potential function. In order for these to be compared with the constant coefficient and its potentials in a homogeneous layer, the WKBJ exponential containing the vertical depth integral is defined as the potential function itself and the remainder is assigned to the variable coefficient. With the potential written in the form

$$\phi(k, z, \omega) = E(z, z_0) \exp\left[\mp \int_{z_0}^{z} \nu_\alpha(x)\, dx\right] \tag{25}$$

$E(z, z_0)$ is the variable coefficient. The first argument, z, of $E(z, z_0)$ indicates the depth position at which the coefficient is evaluated, and the second one is for the reference position of the potential function. If a new reference position z_1 is chosen, the potential becomes

$$\begin{aligned} \phi(k, z, \omega) &= E(z, z_0) \exp\left[\mp \int_{z_0}^{z_1} \nu_\alpha(x)\, dx\right] \exp\left[\mp \int_{z_1}^{z} \nu_\alpha(x)\, dx\right] \\ &= E(z, z_1) \exp\left[\mp \int_{z_1}^{z} \nu_\alpha(x)\, dx\right] \end{aligned} \tag{26}$$

where the new coefficient is

$$E(z, z_1) = E(z, z_0) \exp\left[\mp \int_{z_0}^{z_1} \nu_\alpha(x)\, dx\right].$$

On the other hand, the coefficient E at the reference position $z = z_1$ is

$$\begin{aligned} E(z_1, z_1) &= E(z_1, z_0) \exp\left[\mp \int_{z_0}^{z_1} \nu_\alpha(x)\, dx\right] \\ &= \phi(k, z_1, \omega). \end{aligned} \tag{27}$$

Therefore, the variable coefficient evaluated at a reference position z_1 is actually the potential itself at that depth.

In order to match the coefficients with Haskell's matrix formulation, the variable coefficients are multiplied by the normalization factors $-k^2 \cdot c^2/\alpha^2(z_{\mathrm{ref}})$ for P-wave potentials, and $ik^3/\gamma(z_{\mathrm{ref}})$ for S-wave potentials where $\gamma = 2(\beta^2/c^2)$.

The homogeneous coefficient-equivalents of these WKBJ variable coefficients for the propagator matrix formulation at the boundary of the half-space are

$$\hat{\Delta}_{z_H} = -E_\alpha(z_H, z_H)\left[\frac{kc}{\alpha(z_H)}\right]^2$$
$$\hat{\omega}_{z_H} = E_\beta(z_H, z_H)\frac{ik^3}{\gamma(z_H)} \tag{28}$$

for *P*- and *S*-waves, respectively, where z_H is the depth at the top of the half-space.

A WKBJ-type *S*-wave from an isotropic or dislocation source is assumed to propagate up to the half-space boundary as a direct or turning wave. The coefficients are evaluated at the depth of z_H of the half-space boundary for the *S*-wave potentials.

Including the 'WKBJ' reflection coefficient and equation (28), the coefficient due to an *SV*-wave from an isotropic source is

$$\hat{\omega}''_{0n} = \frac{ik^3}{\gamma_n(z_H)}E(z_H, z_H)$$
$$= -\frac{M_0(\omega)k^4[\exp(-i\omega\tau_D) + i\exp(-i\omega\tau_T)]}{4\pi\beta^2(z_s)\omega\gamma_n(z_H)[\rho(z_H)\rho(z_s)]^{1/2}\eta_\beta^{1/2}(z_s)\eta_\beta^{1/2}(z_H)}. \tag{29}$$

Here the superscript $''$ indicates an upgoing wave, and the subscript n indicates the nth layer, i.e. the half-space. The arguments of exponential terms τ_D and τ_T are defined to be vertical phase times for the direct and turning wave given as

$$\tau_D = \int_{z_H}^{z_s}\eta_\beta(x)\,dx$$
$$\tau_T = 2\int_{z_s}^{z_p}\eta_\beta(x)\,dx + \tau_D. \tag{30}$$

The coefficients for dislocation sources are obtained in an analogous manner using equations (4, 6, 28, 30). They are as follows

$$\hat{\omega}''_{1n} = K(\omega)\frac{k^4}{\gamma_n(z_H)}\frac{\eta_\beta^{1/2}(z_H)}{\eta_\beta^{1/2}(z_s)}[i\exp(-i\omega\tau_D) + \exp(-i\omega\tau_T)]$$
$$\hat{\omega}''_{2n} = -K(\omega)\frac{k^3}{\omega\gamma_n(z_H)\eta_\beta^{1/2}(z_s)\eta_\beta^{1/2}(z_H)}\left[[k_\beta^2(z_H) - k^2]\frac{\eta_\beta(z_s)}{\eta_\beta(z_H)} - k^2\right]$$
$$\times[\exp(-i\omega\tau_D) + i\exp(-i\omega\tau_T)]$$
$$\hat{\omega}''_{3n} = K(\omega)\frac{k^4}{\gamma_n(z_H)}\frac{\eta_\beta^{1/2}(z_s)}{\eta_\beta^{1/2}(z_H)}\left[2 + \frac{\eta_\beta(z_H)}{\eta_\beta(z_s)}\right][i\exp(-i\omega\tau_D) + \exp(-i\omega\tau_T)] \tag{31}$$
$$K(\omega) \equiv -\frac{\mu D(\omega)}{4\pi\omega^2\rho^{1/2}(z_s)}.$$

Here, $\hat{\omega}''_{1n}$, $\hat{\omega}''_{2n}$, and $\hat{\omega}''_{3n}$ are the coefficients for vertical strike-slip, vertical dip-slip, and 45° dip-slip dislocation sources, respectively.

A wave from a source in a stack of homogeneous layers in the source structure arrives at the half-space boundary. From here the wave is assumed to propagate as a WKBJ turning

wave deep in the inhomogeneous media. The wave eventually appears at the boundary of the half-space at the receiver structure. A total of $(n-1)$ and $(n'-1)$ layers are assumed in the source and the receiver structures, respectively, over the inhomogeneous half-space. The depth to these half-space boundaries are z_H and z'_H.

The normalized potential coefficient of a downgoing SV-wave at z_H and an upgoing SV-wave at z'_H are

$$\begin{aligned}\hat{\omega}'_n(z'_H) &= \frac{ik^3}{\gamma_{n'}(z'_H)} E'(z_H, z_H) \\ \hat{\omega}''_{n'}(z'_H) &= \frac{ik^3}{\gamma_{n'}(z'_H)} E''(z'_H, z'_H)\end{aligned} \tag{32}$$

where the definitions of E' and E'' are

$$\begin{aligned}E'(z, z_1) &= \hat{\omega}'^{w}(z_H)\, \eta_\beta^{-1/2}(z) \exp\left[-i\omega \int_{z_H}^{z_1} \eta_\beta(x)\, dx\right] \\ E''(z, z_1) &= \hat{\omega}''^{w}(z_H)\, \eta_\beta^{-1/2}(z) \exp\left[i\omega \int_{z_H}^{z_1} \eta_\beta(x)\, dx\right]\end{aligned} \tag{33}$$

and $\hat{\omega}'^{w}(z_H)$, $\hat{\omega}''^{w}(z_H)$ are the coefficients of the WKBJ potentials of downgoing and upgoing waves at $z = z_H$, respectively.

The amplitude ratio of the upgoing wave to the downgoing wave at z_H is the reflection coefficient

$$R(z_H) = \frac{\hat{\omega}''^{w}(z_H)}{\hat{\omega}'^{w}(z_H)} = i \exp\left[-2i\omega \int_{z_H}^{z_p} \eta_\beta(x)\, dx\right]. \tag{34}$$

From these equations (32–34), the coefficient of the upgoing SV-wave under the half-space boundary at the receiver structure side

$$\hat{\omega}''_{n'}(z'_H) = \hat{\omega}'_n(z_H) \frac{\gamma_n(z_H)\eta_{\beta_n}^{1/2}(z_H)}{\gamma_{n'}(z'_H)\, \eta_{\beta_{n'}}^{1/2}(z'_H)}\, i \exp\left[\left[-i\omega\left[2\int_{z_H}^{z_p} \eta_\beta(x)\, dx - \int_{z_H}^{z'_H} \eta_\beta(x)\, dx\right]\right]\right] \tag{35}$$

is obtained.

In the same way as the S-wave case (and with the normalization factor $-k^2[c/\alpha]^2$) the coefficient for a P-wave becomes

$$\hat{\Delta}''_{n'}(z'_H) = \hat{\Delta}'_n(z_H)\left[\frac{\alpha_n(z_H)}{\alpha_{n'}(z'_H)}\right]^2 \frac{\eta_{\alpha_n}^{1/2}(z_H)}{\eta_{\alpha_{n'}}^{1/2}(z'_H)} \cdot i \exp\left[\left[-i\omega\left[2\int_{z_H}^{z_p} \eta_\alpha(x)\, dx - \int_{z_H}^{z_{H'}} \eta_\alpha(x)\, dx\right]\right]\right]. \tag{36}$$

The computed vertical phase time (i.e. depth integral part of equations (30) or (35–36)) is a complex number to be used as the input data for the WKBJ potential coefficient at the depth of the lowest boundary of the layers. The imaginary part of it is concerned with the amplitude attenuation due to anelasticity. This is comparable to half the ratio of body wave travel time to the average Q value, T/Q, usually used as an approximation in computations for the geometric ray. Therefore, conceptually the imaginary part is not actual time, and only the real part of the vertical phase time is used for the calculation of the horizontal

range that the WKBJ ray reaches. The horizontal propagation range is represented by

$$\Delta(p) = -\frac{d}{dp}\,\mathrm{Real}\,(\tau). \tag{37}$$

Integral representation of displacement

The analysis of the previous sections can be classified as two cases. One is the case of a source in the inhomogeneous half-space and the other is a source in homogeneous layers. In both cases, the vertical and horizontal displacements at the Earth's surface are derived in the wavenumber–frequency domain. From equation (20) vertical and horizontal components of velocities at a receiver are

$$\begin{aligned}\frac{\dot{u}_0}{c} &= -2\frac{\bar{J}_{12}}{R_{11}}\hat{\omega}_n'' \\ \frac{\dot{w}_0}{c} &= 2\frac{\bar{J}_{11}}{R_{11}}\hat{\omega}_n''\end{aligned} \tag{38}$$

assuming no upgoing *P*-wave at the bottom of layers. If the source is in the inhomogeneous half-space, the potential coefficient $\hat{\omega}_n''$ of an upgoing *SV*-wave in equation (38) becomes either $\hat{\omega}_{0n}''$ of an 'isotropic' *SV* source in equation (29), or $\hat{\omega}_{in}''$ ($i = 1, 2, 3$) of dislocation sources in equation (31). $\hat{\omega}_n''$ also represents the potential coefficient $\hat{\omega}_n''(z_H')$ of a turning *SV*-wave (equation 35) travelling from the bottom of layers at the source, if the source is in layers. The coefficient of the downgoing *SV*-wave below layers in source structure is obtained from the matrix equation (18).

In order to obtain the final time series at a field point, the inverse transform from the wavenumber domain to radial distance is done first and the transform from frequency to time next. The transforms are performed by numerical integration along real values of wavenumber and then also by numerical integration over real values of frequency (inverse Fourier transform) in the way of Fuch's reflectivity method (Fuchs 1968a, b; Kind 1978).

The integrals in the wavenumber domain are as follows:

$$\begin{aligned}u(r, \omega) &= -\int \frac{1}{k}\frac{\dot{u}_0}{c} J_1(kr)\,dk \\ w(r, \omega) &= -\int \frac{i}{k}\frac{\dot{w}_0}{c} J_0(kr)\,dk\end{aligned} \tag{39}$$

for the explosion and 'isotropic' shear source, and

$$\begin{aligned}u(r, \theta, \omega) &= -\sum_{n=0}^{2}\int \frac{1}{k}\frac{\dot{u}_0}{c} J_{n+1}(kr)\,dk\,[a_n \cos n\theta + b_n \sin n\theta] \\ w(r, \theta, \omega) &= -\sum_{n=0}^{2}\int \frac{i}{k}\frac{\dot{w}_0}{c} J_n(kr)\,dk\,[a_n \cos n\theta + b_n \sin n\theta]\end{aligned} \tag{40}$$

where,

$$a_0 = \frac{1}{2}\sin\lambda \sin 2\delta \qquad b_0 = 0$$

$$a_1 = \cos\lambda \cos\delta \qquad b_1 = -\sin\lambda \cos 2\delta$$

$$a_2 = \frac{1}{2}\sin\lambda \sin 2\delta \qquad b_2 = \cos\lambda \sin\delta$$

for dislocation sources. Here $n = 0, 1, 2$ are for the cases of 45° dip-slip, vertical dip-slip, and vertical strike-slip, dislocations respectively. The a_i and b_i are source orientation terms. The source orientation angles δ and λ are dip and rake respectively, and θ indicates the azimuth (Fig. 1).

The integral representations of the displacements in equations (39) and (40) are summarized in the form

$$G(r, \omega) = \int F(k, \omega) J_n(kr)\, dk, \qquad n = 0, 1, 2. \tag{41}$$

The integration is limited to a finite slowness p-window rather than wavenumber k-window in order to examine interesting generalized rays with particular incidence angles. A cosine taper is applied to the end points of $F(k, \omega)$ in p-space in order to minimize non-physical diffraction effects caused by the sudden truncation of the kernel. The variation of the kernel $F(k, \omega)$ in the slowness domain is small for the low-frequency case. Therefore, the interval of the sampled slowness p value for numerical calculation of the kernel is taken to be large for low frequencies and the sampling rate is linearly increased with increasing frequency.

The amplitude and phase spectrum of the kernel $F(k, \omega)$ are much simpler in form compared to the real and imaginary components individually. A simple linear phase-curve of the kernel with a steep slope in the phase-slowness space corresponds to rapid oscillations of real and imaginary components of the function which lead to higher-order terms of polynomials in curve-fitting. Taking advantage of this simplicity, a linear interpolation scheme in amplitude and phase is used to reduce the number of calculation points in slowness space. A test for linearity is done before applying interpolation, and the slowness interval of computation of $F(k, \omega)$ is halved successively in the non-linear region until the predefined tolerance value in linearity is met.

Preliminary calculations of the kernel $F(k, \omega)$ are done at a predetermined slowness interval to find an approximate maximum amplitude and to set up blocks for the linearity tests. A block is defined as a region between two adjacent slowness points. It is assumed that the phase difference of the kernel between two end points of a block is less than 180°. In the linearity test the block is halved by a slowness point at the middle of the block. The first test is done using the three values of $F(k, \omega)$ at the middle and end points of the block. The area of the triangle made by three points of these amplitude values of the kernel in the amplitude–slowness space, and the triangular area made by three points of phase values in the phase–slowness space are divided by the slowness interval of the block. The results are approximate error densities of the linearity for the linear curves of the kernel in the block. The error density of amplitude is divided by the maximum amplitude of the spectrum, and the error density of phase is divided by 2π to get relative error densities of linearity. The values of these relative error densities should be smaller than the predetermined tolerance values to meet the linearity test. If the test does not meet the criteria, each half-block becomes a new test block. These new blocks are tested in the same procedures as was done for the original block until the linearity is satisfied.

After linearity of the phase and the amplitude is verified, the phase and amplitude are interpolated linearly in a phase interval between 20 and 30° to get interpolated $F(k, \omega)$ at points in slowness space with uneven slowness intervals.

It was found that the phase interpolation and variable interval technique of sampling was not necessary for every wavenumber integration problem. However it can be usually used to find a proper sampling rate in the p domain for the constant slowness-interval scheme in a specific model case. The linearity test itself requires some additional computation time, and this additional time might be used for the computations of $F(k, \omega)$ at more

points. As long as the proper constant interval of slowness for each frequency is used, the result of the integration is as accurate as the case for a variable interval.

Since teleseismic waves are of primary interest, Hankel's asymptotic expansion (Abramowitz & Stegun 1964) is used for the Bessel function. The integration between adjacent wavenumber points at which the values of the kernel $F(k, \omega)$ are known is done analytically (Apsel 1979) to accommodate the rapid oscillation of the Bessel function in the interval. Finally the Fast Fourier Transform is used to transform the spectra into the time domain.

Validation and comparison

The validation of the current theory and the computational method is established in two steps. First, a computer program was written using Kind's (1978) formulation of the extended reflectivity method with some modifications of the source term and computational

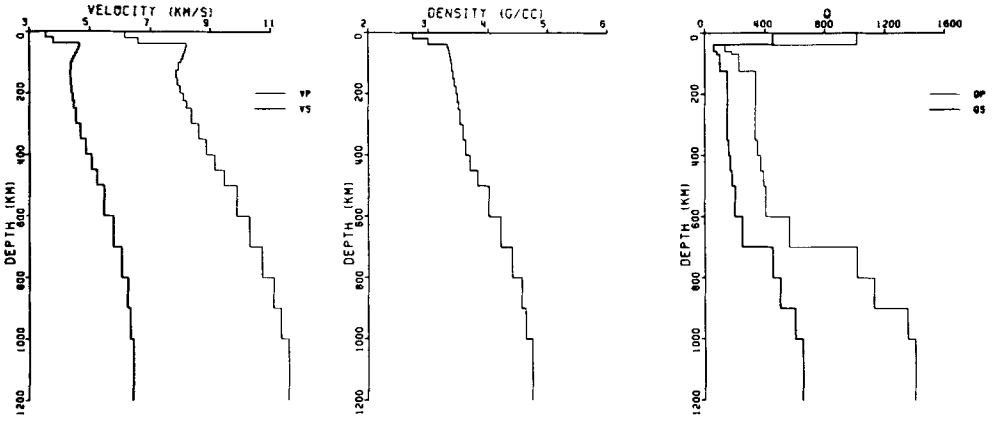

Figure 4. Layered distribution of the Gutenberg–Bullen earth model. (a) Velocity distribution. *VP*: velocity of *P*-wave, *VS*: velocity of *S*-wave. (b) Density distribution. (c) Combined *Q* distribution. *QP*: *Q* of *P*-wave, *QS*: *Q* of *S*-wave.

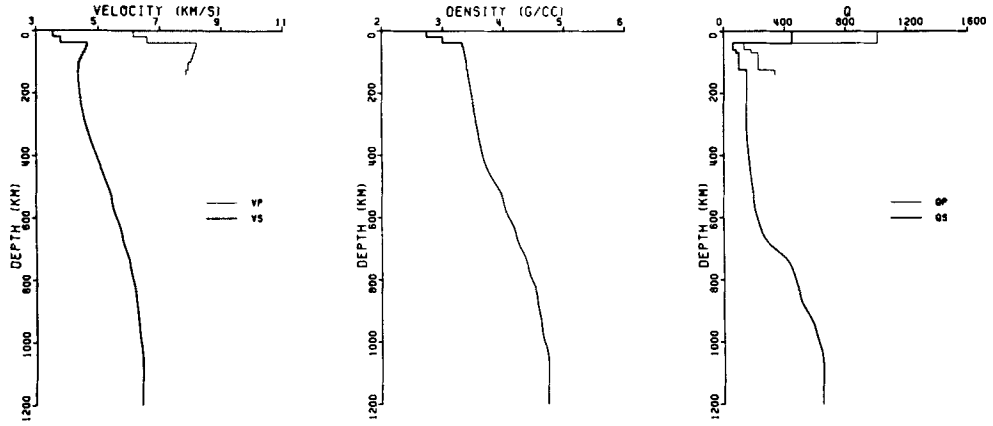

Figure 5. Continuous and layered distribution of the Gutenberg–Bullen earth model. (a) Velocity distribution. *VP*: velocity of *P*-wave, *VS*: velocity of *S*-wave. (b) Density distribution. (c) Combined *Q* distribution. *QP*: *Q* of *P*-wave, *QS*: *Q* of *S*-wave.

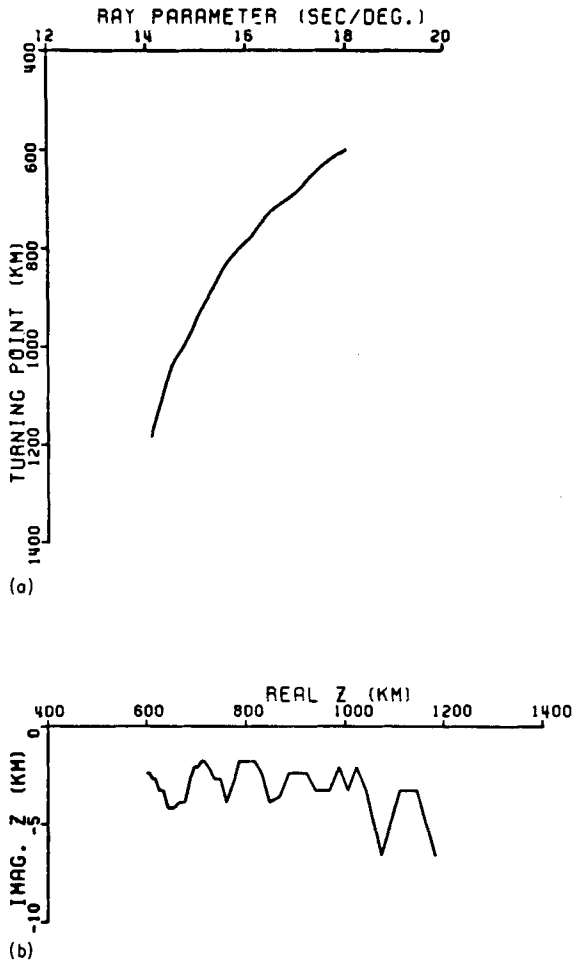

Figure 6. Turning points of WKBJ ray for source depth of 600 km in the Gutenberg–Bullen earth model. (a) Turning point and ray parameter. (b) Real and imaginary components of turning point.

methods. The result of the computation with this program was compared with Apsel's (1979) result. Even though Apsel did not produce *SV*-waves and the comparison was done for a full seismogram of *P*, *S* and Rayleigh waves at short range, the correctness of the formulation and computational method can be proved. Secondly, *S*- and *SPL*-waves were computed using Kind's method, since the extended reflectivity method can generate these waves as well as other seismic phases. These waves were compared with the waves synthesized using the current theory. The disadvantage of the conventional reflectivity method for teleseismic *SV* is the long computation time due to the large number of homogeneous layers required to approximate the model.

Since the extended reflectivity method for homogeneous layers can compute a complete seismogram, synthetic *S*- and *SPL*-waves can be generated by specifying a finite slowness window corresponding to these waves. The *S*- and *SPL*-waves from two different depths of vertical strike-slip sources are produced using the computer program for homogeneous layers for comparison with the synthetics from the combined WKBJ and layer matrix method.

The Gutenberg–Bullen earth model is vertically divided to 24 layers down to the depth of 1200 km (Fig. 4) for the homogeneous layer matrix method. For the combined WKBJ

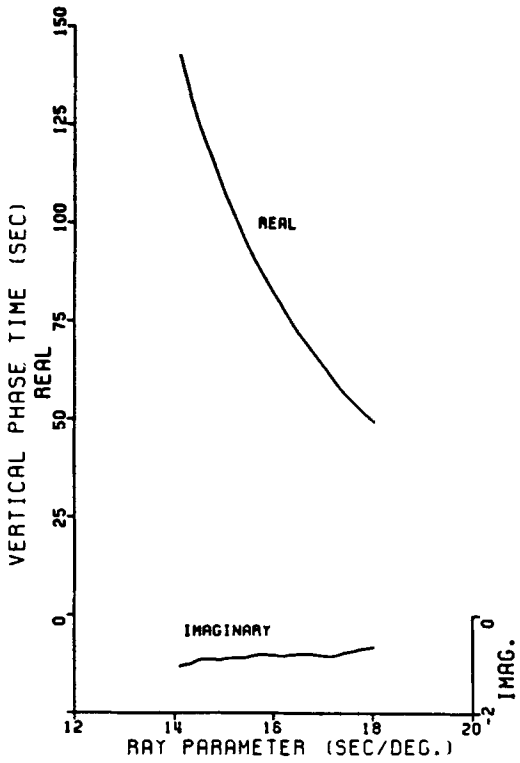

Figure 7. Vertical phase time and ray parameter of the WKBJ ray for source depth 600 km, layer boundary at 140 km, Gutenberg–Bullen earth model.

and layer matrix method, the model is split into two parts, (1) the near-surface layered part down to the depth of 140 km and (2) the smoothed, continuous half-space part below the layer (Fig. 5). The *P*-wave velocity distribution is not plotted at depths below 140 km, since the *SV* WKBJ ray only is assumed at these depths. A reasonable distribution for seismic quality factor Q is added to the model in both cases (Figs 4 and 5). Since the combined WKBJ and layer matrix method is formulated in two ways, with or without the effect of the near-surface source structure, two proposed sources are put at the depth of 600 km in the inhomogeneous half-space and at 15 km depth in the homogeneous layer in order to check both of the formulations.

For the 600 km source depth case, the low and high limits of the ray parameter used for *S* and *SPL* are 14.2 and 17.6 s deg^{-1}, respectively, for both the layer matrix method and the combined WKBJ and layer matrix method. For this case the near-surface source structure is not considered in the computation with the combined WKBJ and layer matrix method. The turning points of the WKBJ ray have real and imaginary parts due to the anelastic attenuation as shown in Fig. 6. The complex vertical phase times of Fig. 7 are used as the input data for the WKBJ potential coefficient at the 140 km depth, the lower boundary of the layers. The range-ray parameter relation and travel times of the WKBJ ray are given in Fig. 8. The function $\exp(-1/t - t/3)H(t)$ for source-time history and the instrument with $T_0 = 30$ s and $T_g = 100$ s (Fig. 9) are used for the final synthetics. Fig 10 displays the comparison of the synthetic radial and vertical component of the *S*- and *SPL*-waves at a 30° range produced by the two methods. Both sets of seismograms are almost identical except for some arrivals of small amplitude in the seismogram from the

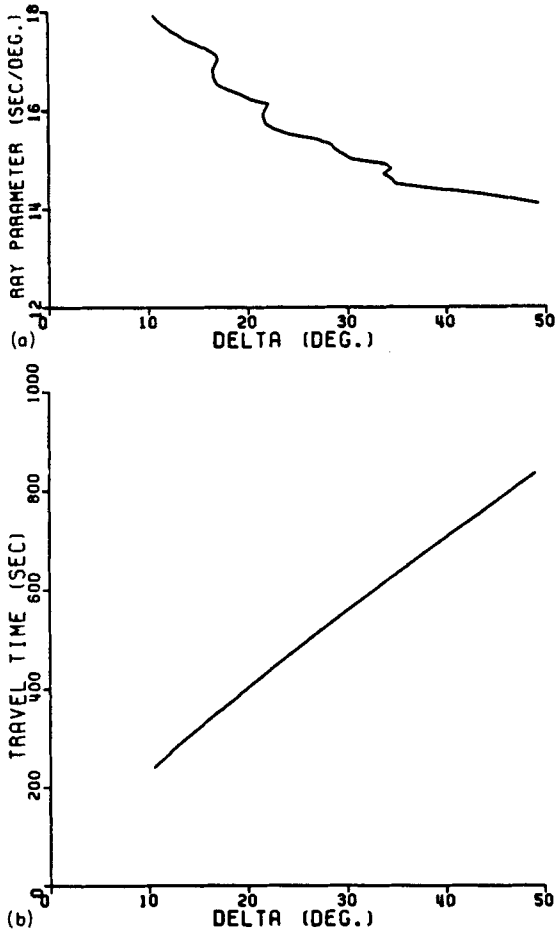

Figure 8. Travel time, ray parameter and range of the WKBJ ray for source depth 600 km, layer boundary at 140 km, Gutenberg–Bullen earth model. (a) Ray parameter and range. (b) Travel time and range.

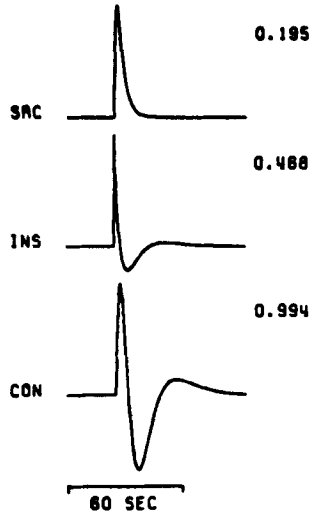

Figure 9. Source time function and instrument response. SRC: source time function $\exp(-1/t - t/3)H(t)$. INS: instrument, $T_0 = 30$ s, $T_g = 100$ s. CON: convolution of source and instrument.

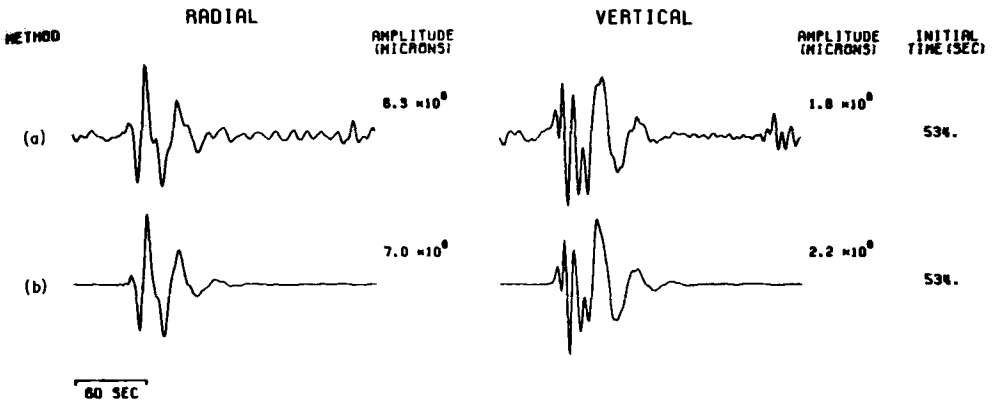

Figure 10. Comparison of synthetic *SV*-waves from the layer matrix method and the combined WKBJ and layer matrix method for vertical strike-slip source at 600 km depth, Gutenberg–Bullen earth model. (a) Layer matrix method of Kind's formulation. (b) Combined WKBJ and layer matrix method (the present method).

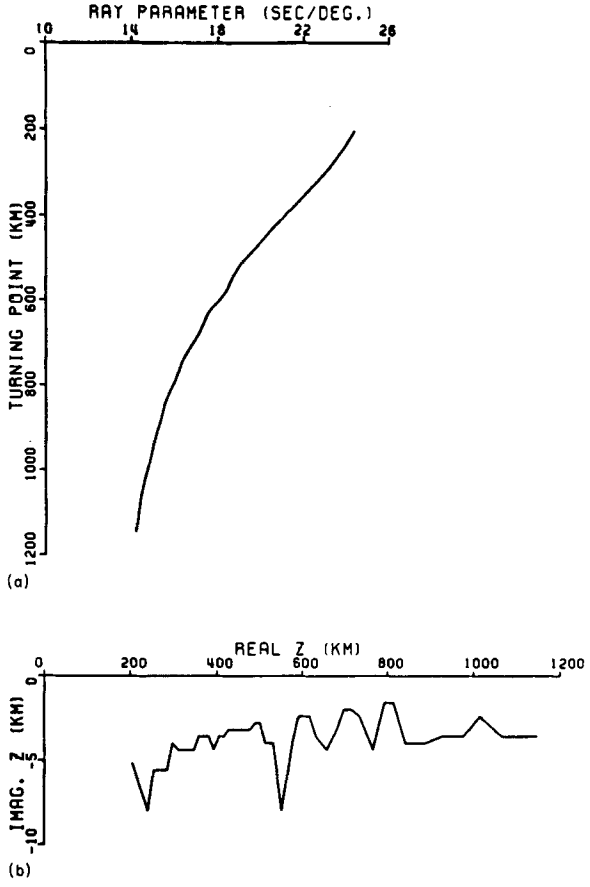

Figure 11. Turning point of WKBJ ray for a source at 15 km in layers with layer boundary at 140 km, Gutenberg–Bullen earth model. (a) Turning point and ray parameter. (b) Real and imaginary components of turning point.

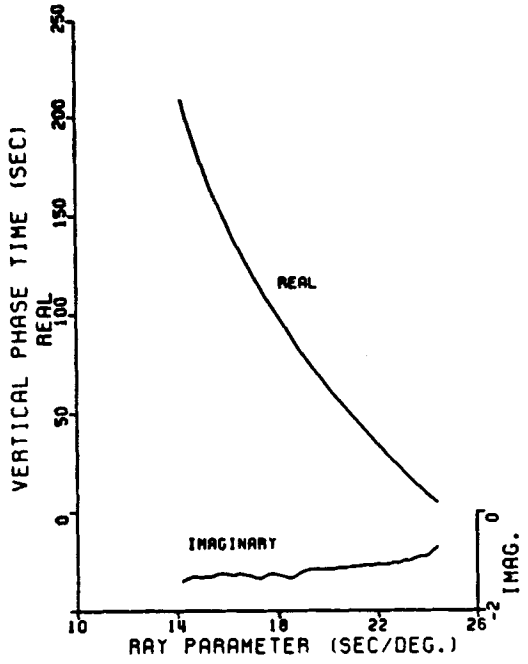

Figure 12. Vertical phase time and ray parameter of WKBJ ray for a source at 15 km in layers with layer boundary at 140 km depth, Gutenberg–Bullen earth model.

homogeneous layer matrix method. These arrivals are interpreted to be caused by the coarse layering in the homogeneous layer model. The first peak and the next trough in the radial component, and the first peak and the next peak in the vertical component are *Sp*- and *S*-waves, respectively.

For the case of a source at 15 km depth in the crust, the near-surface source structure is taken into account in the computation with the combined WKBJ and layer matrix method by taking the lowest boundary of the layers down to a 140 km depth. The ray parameter window is put between 14.3 and 23.8 s deg^{-1}. Figs 11–13 exhibit the information on the WKBJ ray. The computed *S*- and *SPL*-waves from both of the methods, using source and instrument as given in Fig. 9, are compared in Fig. 14. The two seismograms are almost the same.

The good agreement between seismograms shown in those tests proves the validity of the new method for synthesizing the *S*- and *SPL*-waves.

Conclusions

The method of synthesizing *S*- and *SPL*-waves presented here overcomes some of the limitations of the previous methods and should allow for more realistic interpretations of source parameters and velocity structure. The method employs the propagator-matrix technique for waves in near-surface homogeneous layers, and WKBJ theory for a generalized ray in a vertically inhomogeneous half-space below the stack of homogeneous layers. Seismic anelasticity is included by using complex-valued velocity in all regions of the earth model. The near-surface source structure is taken into account in the computation for the case of a shallow source by allowing a point source to be located in the upper layers with appropriate discontinuity conditions in stress and displacement at the source depth. The down-

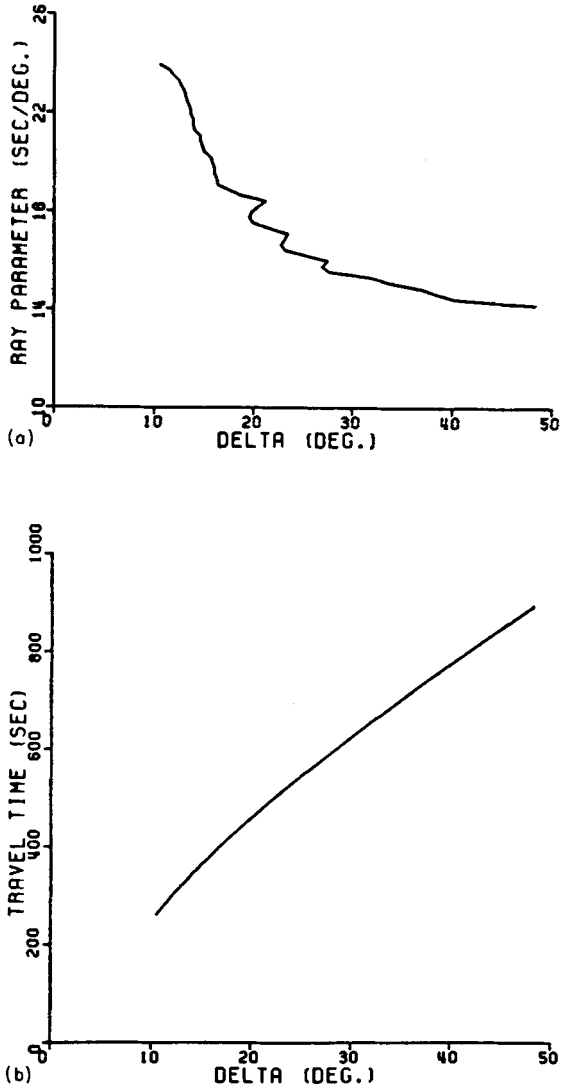

Figure 13. Travel time, ray parameter, and range of WKBJ ray for a source at 15 km in layers with layer boundary at 140 km, Gutenberg–Bullen earth model. (a) Ray parameter and range. (b) Travel time and range.

going shear wave potential coefficient in the half-space, excited by a source in a stack of layers near the surface, which is used here is in a very efficient form for actual numerical computations. All matrix types are separated into half-space, layers below, and layers above the source with no double or triple multiplication of matrix elements in any one layer. The source and receiver structures are allowed to be different. Both dislocation and explosion sources are considered, since the resulting Green's functions can be used for a full moment-tensor source description. Shear wave potentials for dislocation sources in inhomogeneous continuous media obtained by the WKBJ approximation were developed for cylindrical symmetry. The solution is evaluated in the frequency domain by performing a wavenumber integration over a specific range of real wavenumbers, and the result is inverse Fourier transformed to get displacement at the free surface in the time domain.

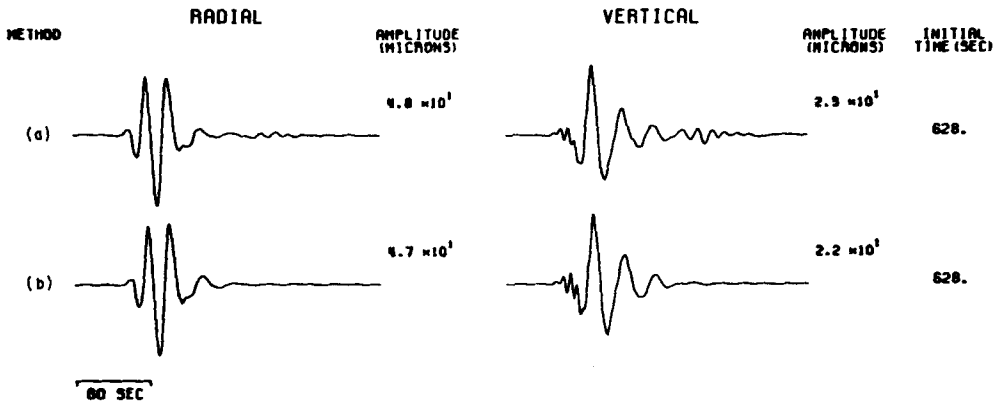

Figure 14. Comparison of synthetic *SV*-waves from the layer matrix method and the combined WKBJ and layer matrix for vertical strike-slip source at 15 km depth, Gutenberg–Bullen earth model. (a) Layer matrix method of Kind's formulation. (b) Combined WKBJ and layer matrix method (the present method).

Computed *SV*-waves using the new method compared favourably with synthetic *SV*-waves produced by Kind's (1978) extended reflectivity method. The reflectivity method is appropriate for homogeneous structure but needs a large computational time because numerous layers are used to simulate continuous layers in the model. The computational time using the new method is reduced to at least one-fifth of that of the reflectivity method for the same accuracy in the teleseismic case.

In the formulation of the theory, the source and receiver structures are allowed to be different since the *SPL*-wave is generated at a teleseismic distance and the property of the *SV*-wave leaking into the mantle in the source side is affected by the source structure for the shallow source; future studies can take advantage of this important capability. A second study will address physical aspects of *SV*- and *SPL*-wave propagation.

Acknowledgments

The authors would like to thank Dr Roy J. Greenfield for his suggestions and discussions in the wavenumber integration technique. This research was supported by the Advanced Research Projects Agency of the Department of Defense and was monitored by the Air Force Office of Scientific Research under Grant AFOSR-82-0054 and Contract F49620-83-K-0019.

References

Abo-Zena, A., 1979. Dispersion function computations for unlimited frequency value, *Geophys. J. R. astr. Soc.*, **58**, 91–105.

Abramowitz, M. & Stegun, I. A., 1964. *Handbook of Mathematical Functions*, Dover, New York.

Aki, K. & Richards, P. G., 1980. *Quantitative Seismology; Theory and Methods, Vol. 1*, W. H. Freeman, San Francisco.

Ando, M., Ishikawa, Y. & Yamazaki, F., 1983. Shear wave polarization anisotropy in the upper mantle beneath Honshu, Japan, *J. geophys. Res.*, **88**, 5850–5864.

Apsel, Randy J., 1979. Dynamic Green's functions for layered media and applications to boundary-value problems, *PhD thesis*, University of California at San Diego.

Baag, C.-E. & Langston, C. A., 1985. Shear-coupled *PL*, *Geophys. J. R. astr. Soc.*, **80**, 363–385.

Bouchon, M., 1981. A simple method to calculate Green's functions for elastic layered media, *Bull. seism. Soc. Am.*, **71**, 959–971.

Budden, K. G., 1961. *Radio Waves in the Ionosphere*, Cambridge University Press.

Burridge, R. & Knopoff, L., 1964. Body force equivalents for seismic dislocations, *Bull. seism. Soc. Am.*, **54**, 1875–1888.

Chapman, C. H., 1973. The earth flattening transformation in body wave theory, *Geophys. J. R. astr. Soc.*, **35**, 55–70.

Chapman, C. H., 1978. A new method for computing synthetic seismograms, *Geophys. J. R. astr. Soc.*, **54**, 481–518.

Choy, G. L., 1977. Theoretical seismograms of core phases calculated by frequency-dependent full wave theory, and their implications, *Geophys. J. R. astr. Soc.*, **51**, 275–311.

Cormier, V. F., 1980. The synthesis of complete seismograms in an earth model composed of radially inhomogeneous layers, *Bull. seism. Soc. Am.*, **70**, 691–716.

Cormier, V. F. & Richards, P. G., 1976. Comments on 'The damping of core waves' by Anthony Quamar and Alfredo Zisenberg, *J. geophys. Res.*, **81**, 3066–3068.

Cormier, V. F. & Richards, P. G., 1977. Full wave theory applied to a discontinuous velocity increase: the inner core boundary, *J. Geophys.*, **43**, 3–22.

Crampin, S., 1977. A review of the effects of anisotropic layering on the propagation of seismic waves, *Geophys. J. R. astr. Soc.*, **49**, 9–27.

Dunkin, J. W., 1965. Computation of model solutions in layered media at high frequencies, *Bull. seism. Soc. Am.*, **55**, 335–358.

Frazer, L. Neil, 1977. Synthesis of shear coupled *PL, PhD thesis*, University of Princeton.

Fuchs, K., 1968a. Das Reflexions-und Transmissionsvermogen eines geschichteten Mediums mit beliebiger Tiefen-Verteilung der elastichen Moduln und der Dichte fur schragen Einfall ebener Wellen, *Z. Geophys.*, **34**, 389–413.

Fuchs, K., 1968b. The reflection of spherical waves from transition zones with arbitrary depth-dependent elastic moduli and density, *J. Phys. Earth*, **16**, 27–41.

Fuchs, K. & Müller, G., 1971. Computation of synthetic seismograms with the reflectivity method and comparison with observations, *Geophys. J. R. astr. Soc.*, **23**, 417–433.

Gilbert, F. & Helmberger, D. V., 1972. Generalized ray theory for a layered sphere, *Geophys. J. R. astr. Soc.*, **27**, 57–80.

Harkrider, D. G., 1964. Surface waves in multi-layered elastic media, part I. Rayleigh and Love waves from buried sources in a multilayered elastic halfspace, *Bull. seism. Soc. Am.*, **54**, 627–679.

Harkrider, D. G., 1970. Surface waves in multilayered elastic media, part II. Higher modes spectra and spectral ratios from point sources in plane layered earth models, *Bull. seism. Soc. Am.*, **60**, 1937–1987.

Harkrider, D. G., 1976. Potentials and displacements for two theoretical seismic sources, *Geophys. J. R. astr. Soc.*, **47**, 97–133.

Harvey, D. J., 1981. Seismogram synthesis using normal mode superposition; the locked mode approximation, *Geophys. J. R. astr. Soc.*, **66**, 37–69.

Haskell, N. A., 1953. Dispersion of surface waves on multilayered media, *Bull. seism. Soc. Am.*, **43**, 17–34.

Haskell, N. A., 1960. Crustal reflection of plane *SH* waves, *J. geophys. Res.*, **65**, 4147–4150.

Haskell, N. A., 1962. Crustal reflection of plane *P* and *SV* waves, *J. geophys. Res.*, **67**, 4751–4767.

Helmberger, D. V., 1968. The crust–mantle transition in the Bering Sea, *Bull. seism. Soc. Am.*, **58**, 179–214.

Kennett, B. L. N., 1980. Seismic waves in a stratified half space – II. Theoretical seismograms, *Geophys. J. R. astr. Soc.*, **61**, 1–10.

Kennett, B. L. N. & Kerry, N. J., 1979. Seismic waves in a stratified halfspace, *Geophys. J. R. astr. Soc.*, **57**, 557–583.

Kind, R., 1978. The reflectivitiy method for a buried source, *J. Geophys.*, **44**, 603–612.

Knopoff, L., 1964. A matrix method for elastic wave problems, *Bull. seism. Soc. Am.*, **54**, 431–438.

Langer, R. E., 1949. The asymptotic solutions of ordinary linear differential equations of the second order with special reference to a turning point, *Trans. Am. math. Soc.*, **67**, 461–490.

Langston, C. A., 1983. Kinematic analysis of strong motion *P* and *SV* waves from the Sterling event, *J. geophys. Res.*, **88**, 3486–3497.

Langston, C. A. & Helmberger, D. V., 1975. A procedure for modeling shallow dislocation sources, *Geophys. J. R. astr. Soc.*, **42**, 117–130.

Masse, R. P., 1981. Review of seismic source models for underground nuclear explosions, *Bull. seism. Soc. Am.*, **71**, 1249–1268.

Mellman, G. R. & Helmberger, D. V., 1978. A modified first-motion approximation for the synthesis of body-wave seismograms, *Geophys. J. R. astr. Soc.*, **54**, 129–140.

Müller, G., 1971. Approximate treatment of elastic body waves in media with spherical symmetry, *Geophys. J. R. astr. Soc.*, **23**, 435–449.

Müller, G., 1977. Earth-flattening approximation for body waves derived from geometric ray theory – improvement, corrections, and range of applicability, *J. Geophys.*, **42**, 429–436.

Pekeris, C. L., Abramovici, Alterman F. & Jarosch, H., 1965. Propagation of a compressional pulse in a layered solid, *Rev. Geophys.*, **3**, 25–47.

Richards, P. G., 1974. Weakly coupled potentials for high frequency elastic waves in continuously stratified media, *Bull. seism. Soc. Am.*, **64**, 1575–1588.

Schwab, F. A. & Knopoff, L., 1972. Fast surface wave free mode computations, in *Methods in Computational Physics, Vol. II*, ed. Bolt, B. A., Academic Press, New York.

Thomson, W. T., 1950. Transmission of eleastic waves through a stratified solid medium, *J. appl. Phys.*, **21**, 89–93.

Wang, C. Y. & Herrman, R. B., 1980. A numerical study of *P*-, *SV*- and *SH*-wave generation in a plane layered medium, *Bull. seism. Soc. Am.*, **70**, 1015–1036.

Watson, T. H., 1970. Fast computation of Rayleigh wave dispersion in a layered halfspace, *Bull. seism. Soc. Am.*, **60**, 161–166.

Wiggins, R. A. & Helmberger, D. V., 1974. Synthetic seismogram computation by expansion in generalized rays, *Geophys. J. R. astr. Soc.*, **37**, 73–90.

Woodhouse, J. H., 1978. Asymptotic results for elastodynamic propagator matrices in plane-stratified and spherically-stratified earth models, *Geophys. J. R. astr. Soc.*, **54**, 263–280.

Appendix A: Green's function for a directional force in a vertically inhomogeneous medium

The Fourier-transformed form of the equation of motion with a directional point source $\bar{f}(x, \omega) = \bar{a}\delta(R)h(\omega)$ is represented by

$$\alpha^2(z)\nabla(\nabla\cdot\bar{u}) - \beta^2(z)\nabla\otimes\nabla\otimes\bar{u} + \omega^2\bar{u} = \frac{h(\omega)}{\rho}\left[\nabla\left(\nabla\cdot\frac{\bar{a}}{4\pi R}\right) - \nabla\otimes\nabla\otimes\frac{\bar{a}}{4\pi R}\right] \tag{A1}$$

in slowly varying vertically inhomogeneous media, where $R = [x^2 + y^2 + (z - z_s)^2]^{1/2}$. With the substitution of Richards' (1974) *P* and *S* vector potentials $\bar{A}_p$ and $\bar{A}_s$ of $\bar{u} = 1/[\rho^{1/2}(z)]\,[\nabla(\nabla\cdot\bar{A}_p) - \nabla\otimes\nabla\otimes\bar{A}_s]$, the equation of motion is decoupled into *P*- and *S*-wave parts

$$\begin{aligned}\nabla^2\bar{A}_p + \frac{\omega^2}{\alpha^2(z)}\bar{A}_p &= \frac{h(\omega)\,\bar{a}}{4\pi\rho_s^{1/2}\alpha_s^2}\frac{1}{R}\\ \nabla^2\bar{A}_s + \frac{\omega^2}{\beta^2(z)}\bar{A}_s &= \frac{h(\omega)\,\bar{a}}{4\pi\rho_s^{1/2}\beta_s^2}\frac{1}{R}.\end{aligned} \tag{A2}$$

Applying scalar potentials A_p and A_s such that $\bar{A}_p = A_p\bar{a}$ and $\bar{A}_s = A_s\bar{a}$, these equations are reduced to

$$\begin{aligned}\nabla^2 A_p + \frac{\omega^2}{\alpha^2(z)}A_p &= \frac{h(\omega)}{4\pi\rho_s^{1/2}\alpha_s^2}\frac{1}{R}\\ \nabla^2 A_s + \frac{\omega^2}{\beta^2(z)}A_s &= \frac{h(\omega)}{4\pi\rho_s^{1/2}\beta_s^2}\frac{1}{R}.\end{aligned} \tag{A3}$$

The Bessel–Fourier transform of these equations removes the r dependence and gives

$$\begin{aligned}\nabla^2 A_p + \omega^2\eta_\alpha^2(z)\,A_p &= \frac{h(\omega)}{4\pi\rho_s^{1/2}\alpha_s^2}\frac{\exp(-k|z - z_s|)}{k}\\ \nabla^2 A_s + \omega^2\eta_\beta^2(z)\,A_s &= \frac{h(\omega)}{4\pi\rho_s^{1/2}\beta_s^2}\frac{\exp(-k|z - z_s|)}{k}\end{aligned} \tag{A4}$$

where the vertical slowness $\eta_v^2(z) = 1/v^2(z) - 1/c^2$.

By using the WKBJ solution

$$\phi = \frac{\exp\left(\mp i\omega \int_{z_p}^{z} \eta_\alpha \, dz\right)}{\eta_\alpha^{1/2}}$$

of the homogeneous differential equation (Budden 1961; Aki & Richards 1980) and applying the method of variation of parameters, the WKBJ solution of

$$\frac{d^2}{dz^2}\phi(k, z, \omega) + \omega^2 \eta_\alpha(z)\,\phi(k, z, \omega) = \delta(z - z_s) \tag{A5}$$

is

$$\begin{aligned}\phi(k, z, \omega) &= -\frac{1}{2}\frac{\exp\left[\mp \int_{z_s}^{z} \nu_\alpha(x)\,dx\right]}{\nu_\alpha^{1/2}(z_s)\,\nu_\alpha^{1/2}(z)} \\ &= \hat{G}_p(k, z, \omega; z_s).\end{aligned} \tag{A6}$$

The first equation of (A4) can be solved using the body force term of the representation theorem and $\hat{G}_p(k, z, \omega; z_s)$.

Let the source term of the equation be

$$S(k, z, \omega; z_s) = \frac{h(\omega)}{4\pi\rho^{1/2}(z_s)\,\alpha^2(z_s)}\,\frac{\exp(-k\,|\,z - z_s\,|)}{k} \tag{A7}$$

then

$$\begin{aligned}A_p(k, z, \omega) &= \int_{-\infty}^{\infty} S(k, z', \omega; z_s)\,\hat{G}_p(k, z, \omega; z')\,dz' \\ &= K \int_{-\infty}^{\infty} \frac{\exp(-k\,|\,z' - z_s\,|)\exp\left[\left[\mp\left[I(z) - I(z')\right]\right]\right]}{\nu_\alpha^{1/2}(z')}\,dz'\end{aligned} \tag{A8}$$

with the negative sign for the downgoing and the positive sign for the upgoing waves in the exponential term. Here,

$$I(z) = \int_{-\infty}^{z} \nu_\alpha(x)\,dx,$$

and

$$K = -\frac{1}{2}\,\frac{h(\omega)}{4\pi\rho^{1/2}(z_s)\,\alpha^2(z_s)\,k\nu_\alpha^{1/2}(z)}.$$

For the case of $z < z_s$, the integrand of equation (A8) is expanded to three terms

$$A_p(k, z, \omega) = K \left[\left[\int_{-\infty}^{z} \frac{\exp\,[k(z' - z_s)]\,\exp\,[-I(z) + I(z_s)]}{\nu_\alpha^{1/2}(z')}\,dz' + \int_{z}^{z_s} \frac{\exp\,[k(z' - z_s)]\,\exp\,[I(z) - I(z')]}{\nu_\alpha^{1/2}(z')}\,dz' + \int_{z_s}^{\infty} \frac{\exp\,[-k(z' - z_s)]\,\exp\,[I(z) - I(z')]}{\nu_\alpha^{1/2}(z')}\,dz'\right]\right]. \tag{A9}$$

With an assumption of slow varying $\nu_\alpha(z)$, such that

$$\frac{d\nu_\alpha(z)}{dz}\Big/\nu_\alpha(z) \approx 0\left(\frac{1}{\alpha^2}\frac{dv(z)}{dz}\right)$$

$$\frac{d}{dz'}\frac{\exp\,[kz' - I(z')]}{\nu^{1/2}(z')[k - \nu(z')]} \approx \frac{\exp\,[kz' - I(z')]}{\nu^{1/2}(z')}, \tag{A10}$$

etc., A_p becomes

$$A_p(k, z, \omega) \cong K\left[\left[\frac{-2\nu_\alpha(z)}{k^2 - \nu_\alpha^2(z)}\frac{\exp\,[k(z - z_s)]}{\nu_\alpha^{1/2}(z)} + \frac{2k}{k^2 - \nu_\alpha^2(z_s)}\frac{\exp\left[\int_{z_s}^{z}\nu_\alpha(x)\,dx\right]}{\nu_\alpha^{1/2}(z_s)}\right]\right].$$

Using the identity $k^2 - \nu_\alpha^2 = k_\alpha^2$, the result is

$$A_p(k, z, \omega) = -\frac{h(\omega)}{4\pi\omega^2\rho^{1/2}(z_s)}\left[\left[-\left[\frac{\alpha(z)}{\alpha(z_s)}\right]^2\frac{\exp\,[k(z - z_s)]}{k} + \frac{\exp\left[\int_{z_s}^{z}\nu_\alpha(x)\,dx\right]}{\nu_\alpha^{1/2}(z_s)\,\nu_\alpha^{1/2}(z)}\right]\right]. \tag{A11}$$

In the same way, the S-wave potential becomes

$$A_s(k, z, \omega) = -\frac{h(\omega)}{4\pi\omega^2\rho^{1/2}(z_s)}\left[\left[-\left[\frac{\beta(z)}{\beta(z_s)}\right]^2\frac{\exp\,[k(z - z_s)]}{k} + \frac{\exp\left[\int_{z_s}^{z}\nu_\beta(x)dx\right]}{\nu_\beta^{1/2}(z_s)\,\nu_\beta^{1/2}(z)}\right]\right]. \tag{A12}$$

The inverse Bessel–Fourier transformed forms of equations (A11) and (A12) are

$$A_p(r, z, \omega) = -\frac{h(\omega)}{4\pi\omega^2\rho^{1/2}(z_s)}\left[\left[-\left[\frac{\alpha(z)}{\alpha(z_s)}\right]^2\frac{1}{R} + \int_0^\infty \frac{k\exp\left[\int_{z_s}^{z}\nu_\alpha(x)dx\right]}{\nu_\alpha^{1/2}(z_s)\,\nu_\alpha^{1/2}(z)}\right]\right]J_0(kr)\,dk$$

$$A_s(r, z, \omega) = -\frac{h(\omega)}{4\pi\omega^2\rho^{1/2}(z_s)}\left[\left[-\left[\frac{\beta(z)}{\beta(z_s)}\right]^2\frac{1}{R} + \int_0^\infty \frac{k\exp\left[\int_{z_s}^{z}\nu_\beta(x)dx\right]}{\nu_\beta^{1/2}(z_s)\,\nu_\beta^{1/2}(z)}\right]\right]J_0(kr)\,dk\,. \tag{A13}$$

Using the vector identity $\nabla \otimes \nabla \otimes A_s = \nabla\nabla\cdot A_s - \nabla^2 A_s$, the displacement can be represented by

$$\bar{u} = \frac{1}{\rho^{1/2}(z)}\left[\nabla\nabla\cdot(\bar{A}_p(r, z, \omega) - \bar{A}_s(r, z, \omega)) + \nabla^2\bar{A}_s(r, z, \omega)\right]. \tag{A14}$$

To reduce (A14) into a simple form, the definition of A_α and A_β given as equation (2) and equation (A13) are used.

$$\bar{A}_p(r, z, \omega) - \bar{A}_s(r, z, \omega) = (A_p - A_s)\,\bar{a}$$
$$= \frac{h(\omega)}{4\pi\omega^2\rho^{1/2}(z_s)}\left[\left[\frac{\alpha(z)}{\alpha(z_s)}\right]^2 - \left[\frac{\beta(z)}{\beta(z_s)}\right]^2 + A_\beta - A_\alpha\right]\bar{a}.$$

Now we assume the Poisson's ratio is almost constant, so that

$$\frac{\alpha(z)}{\alpha(z_s)} - \frac{\beta(z)}{\beta(z_s)} \approx 0.$$

Therefore

$$\bar{A}_p(r, z, \omega) - \bar{A}_s(r, z, \omega) = \frac{h(\omega)}{4\pi\omega^2\rho^{1/2}(z_s)}(A_\beta - A_\alpha)\,\bar{a}. \tag{A15}$$

With the use of equations (A3) and (A13), the second term of equation (A14) becomes

$$\nabla^2\bar{A}_s(r, z, \omega) = \frac{h(\omega)}{4\pi\omega^2\rho^{1/2}(z_s)}\frac{\omega^2}{\beta^2(z)}A_\beta\bar{a}. \tag{A16}$$

By substitution of (A15) and (A16) into (A14), the displacement in vector form

$$\bar{u} = \frac{h(\omega)}{4\pi\omega^2\rho^{1/2}(z_s)\,\rho^{1/2}(z)}\left[\nabla\nabla\cdot(A_\beta - A_\alpha) + \frac{\omega^2}{\beta^2(z)}A_\beta\right]\bar{a} \tag{A17}$$

is obtained.

Using the tensor form of $u_i = G_{ij}a_j$ and $h(\omega) = 1$, we get the Green's function G_{ij} for the directional point force with delta time function and unit strength.

$$G_{ij} = \frac{1}{4\pi\omega^2\rho^{1/2}(z_s)\,\rho^{1/2}(z)}\left[\frac{\partial^2}{\partial x_i\partial x_j}[A_\beta - A_\alpha] + \frac{\omega^2}{\beta^2(z)}A_\beta\delta_{ij}\right].$$

Appendix B: formulae related to the layer matrix

NOTATION

Subscript m: mth layer
ρ_m = density
d_m = thickness
α_m = effective P-wave velocity (refer to equation 23)
β_m = effective S-wave velocity (refer to equation 23)
$\gamma_m = 2[\beta_m/c]^2$
$r^2_{\alpha m} = [c/\alpha_m]^2 - 1$
$r^2_{\beta m} = [c/\beta_m]^2 - 1$
$P_m = kr_{\alpha m}d_m$, $Q_m = kr_{\beta m}d_m$
CP = $\cos P_m$, CQ = $\cos Q_m$
STP = $r_\alpha \sin P_m$, STQ = $r_\beta \sin Q_m$
SDP = $\sin P_m/r_\alpha$, SDQ = $\sin Q_m/r_\beta$

NEW MATRIX FOR HALF-SPACE: $[H_{21}, H_{22}, H_{23}, H_{24}]$

$$H_{21} = (\rho_n \alpha_n^2 \gamma_n r_{\beta n})^{-1}$$
$$H_{22} = (\gamma_n - 1)/(\rho_n \alpha_n^2 \gamma_n^2 r_{\alpha n} r_{\beta n})$$
$$H_{23} = -(\rho_n^2 c^2 \alpha_n^2 \gamma_n^2 r_{\beta n})^{-1}$$
$$H_{24} = (\rho_n^2 c^2 \alpha_n^2 \gamma_n^2 r_{\alpha n} r_{\beta n})^{-1}$$

HASKELL MATRIX

$$A_{11} = A_{44} = \gamma\,\mathrm{CP} + (1-\gamma)\,\mathrm{CQ}$$
$$A_{12} = A_{34} = i[\gamma - 1)\,\mathrm{SDP} + \gamma\,\mathrm{STQ}]$$
$$A_{13} = A_{24} = -(\rho c^2)^{-1}[\mathrm{CP} - \mathrm{CQ}]$$
$$A_{14} = i(\rho c^2)^{-1}[\mathrm{SDP} + \mathrm{STQ}]$$
$$A_{21} = A_{43} = -i[\gamma\,\mathrm{STP} + (\gamma - 1)\,\mathrm{SDQ}]$$
$$A_{22} = A_{33} = (1-\gamma)\,\mathrm{CP} + \gamma\,\mathrm{CQ}$$
$$A_{23} = i(\rho c^2)^{-1}[\mathrm{STP} + \mathrm{SDQ}]$$
$$A_{31} = A_{42} = \rho c^2 \gamma(\gamma - 1)(\mathrm{CP} - \mathrm{CQ})$$
$$A_{32} = i\rho c^2[(\gamma - 1)^2\,\mathrm{SDP} + \gamma^2\,\mathrm{STQ}]$$
$$A_{41} = i\rho c^2[\gamma^2\,\mathrm{STP} + (\gamma - 1)^2\,\mathrm{SDQ}]$$

COMPOUND LAYER MATRIX

$$R_{11} = R_{66} = -2\gamma(\gamma - 1) + (2\gamma^2 - 2\gamma + 1)\,\mathrm{CP}\cdot\mathrm{CQ} - \gamma^2\,\mathrm{STP}\cdot\mathrm{STQ} - (\gamma - 1)^2\,\mathrm{SDP}\cdot\mathrm{SDQ}$$
$$R_{12} = R_{56} = i(\rho c^2)^{-1}[\mathrm{CP}\cdot\mathrm{SDQ} + \mathrm{CQ}\cdot\mathrm{STP}]$$
$$R_{13} = R_{14} = R_{36} = R_{46} = -(\rho c^2)^{-1}[(2\gamma - 1)(1 - \mathrm{CP}\cdot\mathrm{CQ}) + (\gamma - 1)\,\mathrm{SDP}\cdot\mathrm{SDQ} + \gamma\,\mathrm{STP}\cdot\mathrm{STQ})]$$
$$R_{15} = R_{26} = -i(\rho c^2)^{-1}[\mathrm{CQ}\cdot\mathrm{SDP} + \mathrm{CP}\cdot\mathrm{STQ}]$$
$$R_{16} = (\rho c^2)^{-2}[2(1 - \mathrm{CP}\cdot\mathrm{CQ}) + \mathrm{STP}\cdot\mathrm{STQ} + \mathrm{SDP}\cdot\mathrm{SDQ}]$$
$$R_{21} = R_{65} = i(\rho c^2)[(\gamma - 1)^2\,\mathrm{CQ}\cdot\mathrm{SDP} + \gamma^2\,\mathrm{CP}\cdot\mathrm{STQ}]$$
$$R_{22} = R_{55} = \mathrm{CP}\cdot\mathrm{CQ}$$
$$R_{23} = R_{24} = R_{35} = R_{45} = i[(\gamma - 1)\,\mathrm{CQ}\cdot\mathrm{SDP} + \gamma\,\mathrm{CP}\cdot\mathrm{STQ}]$$
$$R_{25} = \mathrm{SDP}\cdot\mathrm{STQ}$$
$$R_{31} = R_{41} = R_{63} = R_{64} = (\rho c^2)[\gamma(\gamma - 1)(2\gamma(\gamma - 1)(1 - \mathrm{CP}\cdot\mathrm{CQ}) + (\gamma - 1)^3\,\mathrm{SDP}\cdot\mathrm{SDQ} + \gamma^3\,\mathrm{STP}\cdot\mathrm{STQ}]$$
$$R_{32} = R_{42} = R_{53} = R_{54} = -i[(\gamma - 1)\,\mathrm{CP}\cdot\mathrm{SDQ} + \gamma\,\mathrm{CQ}\cdot\mathrm{STP}]$$
$$R_{33} = R_{44} = 1 + 2\gamma(\gamma - 1)(1 - \mathrm{CP}\cdot\mathrm{CQ}) + (\gamma - 1)^2\,\mathrm{SDP}\cdot\mathrm{SDQ} + \gamma^2\,\mathrm{STP}\cdot\mathrm{STQ}$$
$$R_{34} = R_{43} = R_{33} - 1$$
$$R_{51} = R_{62} = -i(\rho c^2)[(\gamma - 1)^2\,\mathrm{CP}\cdot\mathrm{SDQ} + \gamma^2\,\mathrm{CQ}\cdot\mathrm{STP}]$$
$$R_{52} = \mathrm{STP}\cdot\mathrm{SDQ}$$
$$R_{61} = (\rho c^2)^2[2\gamma^2(\gamma - 1)^2(1 - \mathrm{CP}\cdot\mathrm{CQ}) + (\gamma - 1)^4\,\mathrm{SDP}\cdot\mathrm{SDQ} + \gamma^4\,\mathrm{STP}\cdot\mathrm{STQ}]$$

INVERSE OF HASKELL'S HALF-SPACE MATRIX

$$E_{11}^{-1} = -2[\beta_n/\alpha_n]^2 \qquad E_{13}^{-1} = (\rho_n \alpha_n)^{-1}$$
$$E_{22}^{-1} = c^2(\gamma_n - 1)/(\alpha_n^2 r_{\alpha n}) \qquad E_{24}^{-1} = [\rho_n \alpha_n^2 r_{\alpha n}]^{-1}$$
$$E_{31}^{-1} = (\gamma_n - 1)/(\gamma_n r_{\beta n}) \qquad E_{33}^{-1} = -(\rho_n c^2 \gamma_n r_{\beta n})^{-1}$$
$$E_{42}^{-1} = 1 \qquad E_{44}^{-1} = (\rho_n c^2 \gamma_n)^{-1}$$
$$E_{12}^{-1} = E_{14}^{-1} = E_{21}^{-1} = E_{23}^{-1} = E_{32}^{-1} = E_{34}^{-1} = E_{41}^{-1} = E_{43}^{-1} = 0$$

$\bar{\mathbf{E}}$ matrix: $\bar{\mathbf{E}} = \begin{bmatrix} E_{11}^{-1}, & -E_{22}^{-1}, & E_{13}^{-1}, & -E_{24}^{-1} \\ -E_{31}^{-1}, & E_{42}^{-1}, & -E_{33}^{-1}, & E_{44}^{-1} \end{bmatrix}$

$\mathbf{J}$ matrix: $\mathbf{J} = \mathbf{E}^{-1}\mathbf{A}$

$\bar{\mathbf{J}}$ matrix: $\bar{\mathbf{J}} = \bar{\mathbf{E}}\mathbf{A}$

$$\begin{bmatrix} \bar{J}_{11}, & \bar{J}_{12}, & \bar{J}_{13}, & \bar{J}_{14} \\ \bar{J}_{21}, & \bar{J}_{22}, & \bar{J}_{23}, & \bar{J}_{24} \end{bmatrix} = \begin{bmatrix} J_{11} - J_{21}, & J_{12} - J_{22}, & J_{13} - J_{23}, & J_{14} - J_{24} \\ J_{41} - J_{31}, & J_{42} - J_{32}, & J_{43} - J_{33}, & J_{44} - J_{34} \end{bmatrix}$$

SOURCE DISCONTINUITY MATRIX

(1) Dislocation source

$$\delta^2 = \frac{M_0(\omega)}{4\pi} \begin{bmatrix} 0 \\ 0 \\ 0 \\ 2k^2 i \end{bmatrix} \quad \text{for vertical strike-slip}$$

$$\delta^1 = \frac{M_0(\omega)}{4\pi} \begin{bmatrix} -\dfrac{2k^2}{\rho_s \beta_s^2} \\ 0 \\ 0 \\ 0 \end{bmatrix} \quad \text{for vertical dip-slip}$$

$$\delta^0 = \frac{M_0(\omega)}{4\pi} \begin{bmatrix} 0 \\ \dfrac{4k^2}{\rho \alpha_s^2} i \\ 0 \\ -2k^2 \left(4 \dfrac{\beta_s^2}{\alpha_s^2} - 3 \right) i \end{bmatrix} \quad \text{for } 45^\circ \text{ dip-slip.}$$

Here M_0 is the seismic moment.

(2) Explosion source

$$\delta = \frac{i \bar{P}_s a_s^3 \exp(i k_{\alpha_s} a_s)}{4\beta_s^2 \rho_s [1 - (k_{\beta_s} a_s/2)^2 + i k_{\alpha_s} a_s]} \begin{bmatrix} 0 \\ 2k^2 \\ 0 \\ -4k^2 \rho_s \beta_s^2 \end{bmatrix}$$

where a_s = radius of source cavity,
$\bar{P}_s$ = pressure in the cavity.

MATRIX FORMULATIONS OF PARTICLE VELOCITIES $\dot{u}_0$ AND $\dot{w}_0$

From the matrix equation (10), a matrix **X**

$$\begin{bmatrix} X_1 \\ X_2 \\ X_3 \\ X_4 \end{bmatrix} = \begin{bmatrix} \dot{u}_0/c \\ \dot{w}_0/c \\ 0 \\ 0 \end{bmatrix} + \begin{bmatrix} D_1 \\ D_2 \\ D_3 \\ D_4 \end{bmatrix}$$

is defined for convenience to solve the equation. From this we get

$$\dot{u}_0/c = X_1 - D_1$$

$$\dot{w}_0/c = X_2 - D_2$$

$$X_3 = D_3$$

$$X_4 = D_4.$$

Here X_3 and X_4 are solved in terms of D_3 and D_4. The substitution of X in equation (10) gives

$$\begin{bmatrix} \hat{\Delta}'_n \\ \hat{\Delta}'_n \\ \hat{w}'_n \\ \hat{w}'_n \end{bmatrix} = \begin{bmatrix} J_{11}X_1 + J_{12}X_2 + J_{13}D_3 + J_{14}D_4 \\ J_{21}X_1 + J_{22}X_2 + J_{23}D_3 + J_{24}D_4 \\ J_{31}X_1 + J_{32}X_2 + J_{33}D_3 + J_{34}D_4 \\ J_{41}X_1 + J_{42}X_2 + J_{43}D_3 + J_{44}D_4 \end{bmatrix}.$$

These simultaneous equations are solved for X_1 and X_2 by subtraction of the elements of two rows. The result gives

$$X_1 = \frac{1}{\det}\left[\begin{vmatrix} J_{12} - J_{22}, & J_{13} - J_{23} \\ J_{42} - J_{32}, & J_{43} - J_{33} \end{vmatrix} D_3 + \begin{vmatrix} J_{12} - J_{22}, & J_{14} - J_{24} \\ J_{42} - J_{32}, & J_{44} - J_{34} \end{vmatrix} D_4\right]$$

$$X_2 = -\frac{1}{\det}\left[\begin{vmatrix} J_{11} - J_{21}, & J_{13} - J_{23} \\ J_{41} - J_{31}, & J_{43} - J_{33} \end{vmatrix} D_3 + \begin{vmatrix} J_{11} - J_{21}, & J_{14} - J_{24} \\ J_{41} - J_{31}, & J_{44} - J_{34} \end{vmatrix} D_4\right]$$

where

$$\det = \begin{vmatrix} J_{11} - J_{21}, & J_{12} - J_{22} \\ J_{41} - J_{31}, & J_{42} - J_{32} \end{vmatrix}.$$

The substitution of elements of the $\bar{\mathbf{J}}$ matrix results in

$$X_1 = \frac{1}{\det}\left[\begin{vmatrix} \bar{J}_{12}, & \bar{J}_{13} \\ \bar{J}_{22}, & \bar{J}_{23} \end{vmatrix} D_3 + \begin{vmatrix} \bar{J}_{12}, & \bar{J}_{14} \\ \bar{J}_{22}, & \bar{J}_{24} \end{vmatrix} D_4\right]$$

$$X_2 = -\frac{1}{\det}\left[\begin{vmatrix} \bar{J}_{11}, & \bar{J}_{13} \\ \bar{J}_{21}, & \bar{J}_{23} \end{vmatrix} D_3 + \begin{vmatrix} \bar{J}_{11}, & \bar{J}_{14} \\ \bar{J}_{21}, & \bar{J}_{24} \end{vmatrix} D_4\right]$$

and

$$\det = \begin{vmatrix} \bar{J}_{11}, & \bar{J}_{12} \\ \bar{J}_{21}, & \bar{J}_{22} \end{vmatrix} .$$

Using the Dunkin's formulation R_{ij} (equation 12), the solutions are transformed to

$$X_1 = \frac{1}{R_{11}} (R_{13}D_3 + R_{15}D_4)$$

$$X_2 = -\frac{1}{R_{11}} (R_{12}D_3 + R_{13}D_4)$$

where $R_{14} = R_{13}$ is used.

Inserting the solutions X_1, X_2, X_3, and X_4 to the definition of **X** matrix, we get

$$\frac{\dot{u}_0}{c} = \frac{1}{R_{11}} (R_{13}D_3 + R_{15}D_4) - D_1$$

$$\frac{\dot{w}_0}{c} = -\frac{1}{R_{11}} (R_{12}D_3 + R_{13}D_4) - D_2.$$